The Triple-Repeat Protein Anakonda Controls Epithelial Tricellular Junction Formation in Drosophila

Byri, Sunitha ; Misra, Tvisha ; Syed, Zulfeqhar A ; Bätz, Tilmann ; Shah, Jimit ; Boril, Lukas ; Glashauser, Jade ; Aegerter-Wilmsen, Tinri ; Matzat, Till ; Moussian, Bernard ; Uv, Anne ; Luschnig, Stefan

Abstract: In epithelia, specialized tricellular junctions (TCJs) mediate cell contacts at three-cell vertices. TCJs are fundamental to epithelial biology and disease, but only a few TCJ components are known, and how they assemble at tricellular vertices is not understood. Here we describe a transmembrane protein, Anakonda (Aka), which localizes to TCJs and is essential for the formation of tricellular, but not bicellular, junctions in Drosophila. Loss of Aka causes epithelial barrier defects associated with irregular TCJ structure and geometry, suggesting that Aka organizes cell corners. Aka is necessary and sufficient for accumulation of Gliotactin at TCJs, suggesting that Aka initiates TCJ assembly by recruiting other proteins to tricellular vertices. Aka's extracellular domain has an unusual tripartite repeat structure that may mediate self-assembly, directed by the geometry of tricellular vertices. Conversely, Aka's cytoplasmic tail is dispensable for TCJ localization. Thus, extracellular interactions, rather than TCJ-directed intracellular transport, appear to mediate TCJ assembly.

DOI: https://doi.org/10.1016/j.devcel.2015.03.023

The triple-repeat protein Anakonda controls epithelial tricellular junction formation in *Drosophila*

Sunita Byri[1, *], Tvisha Misra[5, *], Zulfeqhar A. Syed[1], Tilmann Bätz[5], Jimit Shah[5], Lukas Boril[5], Jade Glashauser[5], Tinri Aegerter-Wilmsen[5], Till Matzat[3, 4], Bernard Moussian[2], Anne Uv[1, $] and Stefan Luschnig[3, 4, 5, $]

[1]: Institute of Biomedicine, University of Gothenburg, Medicinaregatan 9A, 40530 Gothenburg, Sweden

[2]: Interfaculty Institute for Cell Biology, University of Tübingen, Auf der Morgenstelle 28, 72076 Tübingen, Germany

[3]: Institute of Neurobiology, University of Münster, Badestrasse 9, 48149 Münster, Germany

[4]: Cluster of Excellence EXC 1003, Cells in Motion, CiM, 48149 Münster, Germany

[5]: Institute of Molecular Life Sciences, University of Zürich, Winterthurerstrasse 190, 8057 Zürich, Switzerland

*: These authors contributed equally

[$]: Corresponding authors

Contact:

e-mail: anne.uv@gu.se

e-mail: luschnig@uni-muenster.de

Running title Anakonda controls tricellular junction assembly

Key words Tricellular junction, septate junction, tight junction, epithelial barrier, cell adhesion, epithelial morphogenesis, *Drosophila melanogaster*.

Summary

In epithelia, specialized tricellular junctions (TCJs) mediate cell contacts at three-cell vertices. TCJs are fundamental to epithelial biology and disease, but only few TCJ components are known and how they assemble at tricellular vertices is not understood. Here we describe a transmembrane protein, Anakonda (Aka), which localizes to TCJs and is essential for the formation of tricellular, but not of bicellular junctions in *Drosophila*. Loss of Aka causes epithelial barrier defects associated with irregular TCJ structure and geometry, suggesting that Aka organizes cell corners. Aka is necessary and sufficient for accumulation of Gliotactin at TCJs, suggesting that Aka initiates TCJ assembly by recruiting other proteins to tricellular vertices. Aka's extracellular domain has an unusual tripartite repeat structure that may mediate self-assembly, directed by the geometry of tricellular vertices. Conversely, Aka's cytoplasmic tail is dispensable for TCJ localization. Thus, extracellular interactions, rather than TCJ-directed intracellular transport, appear to mediate TCJ assembly.

Introduction

Epithelial cells are linked via intercellular junctions that provide paracellular diffusion barriers, maintenance of polarity and cell-to-cell communication. Bicellular junctions (BCJs) make up the most abundant intercellular contacts in epithelia. They connect two neighboring plasma membranes and are organized into distinct complexes along the apical-basal axis, collectively forming the apical junctional belt. However, at certain positions along the cell perimeter, three cell-corners meet and the bicellular junctional complex is disjointed. Here, specialized tricellular junctions (TCJs) connect epithelial cells (Staehelin, 1973; Fristrom, 1982; Graf et al., 1982; Noirot-Timothee et al., 1982). TCJs play important roles in epithelial barrier functions (Ikenouchi et al., 2005; Riazuddin et al., 2006; Krug et al., 2009; Furuse et al., 2014) and cytoskeletal organization (Oda et al., 2014), and are preferential sites for trans-endothelial migration of neutrophils (Burns et al., 1997) and metastatic cancer cells (Nakai et al., 2005), as well as for the spreading of intracellular pathogens (Fukumatsu et al., 2012).

Due to the geometry of three-cell vertices, the sealing of the epithelium at these sites requires a dedicated junctional organization. Ultrastructural analyses using freeze-fracture electron microscopy (EM) showed that the zonula occludens, tight junctions (TJs) in vertebrates and septate junctions (SJs) in arthropods (Furuse and Tsukita, 2006; Banerjee et al., 2008), changes characteristics when approaching a three-cell vertex. Instead of continuing parallel to the epithelial plane around the cell perimeter, the junctional strands extend basally, forming a bicellular seal along the apical-basal axis (Staehelin, 1973). In vertebrates, these structures are termed central sealing elements, and three such parallel TJ extensions enclose a narrow (approx. 10 nm) central canal at each TCJ (Staehelin, 1973). Similarly, in invertebrates the SJ strands turn by 90 degrees when approaching a tricellular corner, forming three parallel limiting strands that surround the tricellular juncture space, resembling the central sealing element in vertebrates (Noirot-Timothee and Noirot, 1980; Fristrom, 1982; Graf et al., 1982; Noirot-Timothee et al., 1982). Within and perpendicular to the vertical juncture space are a series of diaphragms, which appear linked not only to three limiting septa, but also to the three cell corner membranes, thereby forming true tricellular contacts (Fristrom, 1982; Graf et al., 1982; Noirot-Timothee et al., 1982).

Despite the fundamental biological importance of TCJs, only few of their components are known (Furuse et al., 2014), and the mechanism of their localized assembly at three-cell vertices is not understood. In vertebrates, the Occludin family protein Tricellulin localizes to TCJs (Ikenouchi et al., 2005) and is recruited there by lipolysis-stimulated lipoprotein receptor (LSR) and related proteins (ILDR1 and ILDR2; Masuda et al., 2011; Higashi et al., 2013). Additionally, the cytoplasmic PDZ-domain-containing protein Tjp2iso3 associates with Tricellulin in Sertoli cells (Chakraborty et al., 2014). The Neuroligin-like transmembrane protein Gliotactin in *Drosophila* is the only TCJ protein characterized so far in invertebrates (Schulte et al., 2003). It is not clear what kind of cues direct the accumulation of these proteins at tricellular vertices, and the features of known TCJ proteins do not explain the distinct structure of three-cell contacts observed by EM. Here, we describe a

transmembrane protein, Anakonda (Aka), which accumulates at TCJs in *Drosophila* epithelia. Aka can initiate TCJ assembly, and may do so through its large extracellular domain, which exhibits an unusual triple-repeat structure.

Results

anakonda mutants develop over-elongated tracheae and epithelial barrier defects

In a mutagenesis screen we isolated an embryonic lethal complementation group with nine alleles that showed excessively elongated tracheal tubes (Figure 1A, B). We named the locus *anakonda* (*aka*) based on the tortuous tube phenotype. In addition, *aka* mutants showed reduced levels of the secreted protein Vermiform-RFP (Verm-RFP; Forster et al., 2010) in the tracheal lumen (Figure 1A, B). These phenotypes are characteristic for mutants lacking epithelial barrier function due to mutations in SJ components (Behr et al., 2003; Paul et al., 2003; Wu et al., 2004). To assess epithelial barrier function, we injected Rhodamine-labeled dextran (10 kDa) into the hemocoel of stage 16 *aka* and control embryos, and followed the distribution of fluorescent signals. While dextran was largely excluded from lumina of hindgut, salivary glands, and tracheae in wild-type embryos (Figure 1F), dextran was readily detectable in the lumina of these organs in *aka* embryos 20 minutes after injection (Figure 1G), indicating that epithelial barrier function was defective.

Besides these defects, stage 17 *aka* embryos showed "cavities" in the tracheal epithelium, seen as round areas, 0.5-6 µm in diameter, from which cytoplasmic GFP was excluded (Figure 1H, I). Similar structures were evident in the epidermis of *aka* embryos. EM analyses revealed that the cavities are lined by two lateral plasma membranes, indicating that they form between neighboring cells (Figure 1J, K), reminiscent of delaminations previously observed in embryos that lack the TCJ protein Gli (Schulte et al., 2003). As SJs were observed on either side of the paracellular cavities, they appear associated with focal loss of cell-cell adhesion.

anakonda encodes a large transmembrane protein with a tripartite extracellular domain

We mapped the *aka* locus and identified a lethal PBac insertion ($PBac^{YD1046}$; Quinones-Coello et al., 2007) in the *CG3921* gene that failed to complement *aka* alleles. Furthermore, tracheal-specific knockdown of *CG3921* by RNAi led to over-elongated tracheae and reduced luminal Verm-RFP levels, resembling the *aka* loss-of-function phenotype (Figure 1C; Jaspers et al., 2012), whereas tracheal-specific expression of a UAS-*aka* transgene rescued the tracheal defects of *aka* embryos (Figure 1D). We conclude that *aka* mutations affect the *CG3921* gene, which we refer to as *aka*.

Three annotated *aka* transcripts yield two protein isoforms of 3115 and 3123 amino acids (aa; Figure 2A), which share an N-terminal signal peptide, a large extracellular domain (2674 or 2682 aa), a transmembrane domain, and an intracellular domain (384 aa) with a class-I PDZ-binding motif (ETAM) at the C-terminus (Figure 2B). Domain prediction using Simple Modular Architecture

Research Tool (SMART; Schultz et al., 1998) indicated three Scavenger Receptor (SR) cysteine rich domains, a Complement/UEGF/BMP1 (CUB) domain, a C-type lectin domain, and nineteen parallel beta-helix (PBH) motifs in the extracellular part. However, in sequence homology searches, parts of the extracellular domain self-aligned over three non-overlapping regions that extend beyond the three annotated SR domains. To explore if Aka might contain extended internal repeats, we retrieved multiple protein alignments of Aka homologues from fourteen species and used profile hidden Markov models (HMM; http://hmmer.janelia.org/) based on these alignments to search for similarities (Figure S1). We found that an 816 aa profile-HMM targets three successive regions of *D. melanogaster* Aka that we term regions I-III (Figure 2C). While region I aligns to the entire profile-HMM, regions II and III each display a single central gap in the alignment of 248 and 289 aa, respectively. Protein structure predictions (Phyre; Kelley and Sternberg, 2009) suggested that region II and III both exhibit a CUB-like fold (confidence >90%), similar to the annotated CUB domain in the central part of region I. In addition, each of the three regions shares a predicted scavenger-receptor-like fold at the N-terminus and a single-stranded right-handed beta-helix motif at the C-terminus (Figure 2C). Together, these analyses predict three tandem repeat regions that together span approximately 2500 of the 2691 aa long extracellular domain. Strikingly, the pattern and spacing of the three repeats and the overall size of the extracellular domain are conserved between Aka homologues from diverse invertebrates and a cephalochordate, suggesting they are of functional importance (Figure S1). The cytoplasmic portion contains no conserved domains, but the C-terminal PDZ-binding motif is conserved among Aka homologues in insects and nematodes. Thus, Aka is a conserved transmembrane protein whose extracellular part comprises an unusual tripartite structure.

aka mutations affect the extracellular part of Aka

We identified mutations in the *aka* coding region in seven EMS-induced *aka* alleles (Figure 2A, B). Three alleles carry mutations that cause C-terminal truncations in the extracellular part. aka^{L200} contains a 128-bp deletion in the third coding exon, resulting in a frame shift and a premature stop codon six codons thereafter. The predicted protein product (587 aa) is truncated after the CUB domain in region I. aka^{N43} contains a G to A transition in the 5' splice site of intron 9. Retention of the intron and translation of the mutant mRNA results in a premature stop codon in region III, yielding a predicted truncated protein of 2394 aa. aka^{J219} contains a premature stop codon (W1579*) in region II. Four *aka* alleles contain missense mutations in the extracellular part, each leading to a single amino acid exchange in region I (aka^{K93}, E678K; aka^{J55}, V567E; aka^{K104}, S680L; aka^{L224}, V503E). Thus, all of the identified EMS-induced *aka* mutations affect the extracellular part of the protein.

We raised antisera against a peptide located in the cytoplasmic domain (Figure 2B). On immunoblots, a band well above 250 kDa was detected in extracts from wild-type embryos, but not from *Df(2L)BSC171* homozygotes, suggesting that this band represents full-length Aka protein (predicted molecular weight (MW) 350 kDa; Figure 2D). Two additional bands of lower MW (around 150 kDa)

may represent proteolytic cleavage products. Electrophoretic mobility of the three Aka species was the same under reducing and non-reducing conditions (Figure 2E), indicating that they are not linked by disulphide bridges. However, treatment of extracts with N-glycanase caused a mobility shift of all three species, suggesting that they are N-glycosylated (Figure 2E). The MW of the smaller species (below 150 kDa) suggests cleavage beyond residue 1800. Trypsin digestion and peptide identification by LC-MS/MS of the smaller species yielded six peptides that cover amino acids 1898 to 3085, arguing that cleavage occurs between extracellular repeats II and III (between residues 1800-1898; Figure 2B, C). In *aka* mutants predicted to produce C-terminally truncated proteins (aka^{L200}, aka^{N43}, aka^{J219}), none of the three specific bands was detectable, whereas the four *aka* alleles with missense mutations in repeat I (aka^{J55}, aka^{L224}, aka^{K93}, aka^{K104}) produced full-length Aka and little if any cleavage products (Figure 2D). Since full-length Aka in *aka* missense mutants showed similar mobility as in wild-type embryos, these mutations appear not to prevent initial steps of N-glycosylation, but preclude the apparent proteolytic processing of Aka.

Aka accumulates at epithelial tricellular junctions

In situ hybridization revealed *aka* expression in ectodermal epithelia (epidermis, foregut, hindgut, salivary glands, tracheae; Figure 2F-H, L) from stage 13. Expression in epithelia declined from late stage 15 (Figure 2I) and *aka* transcripts appeared in the central nervous system (CNS) during stage 16 (Figure 2J, K). This expression pattern resembles those of SJ components that participate in epithelial and blood-brain-barrier functions.

Consistent with transcript analyses, Aka protein was detectable by immunostaining in embryonic epithelia and CNS (Figure 3; Figure S2) of wild-type, but not aka^{L200} embryos (Figure 3B, G). Moreover, a genomic Aka transgene carrying a Ty1-Tev-SGFP-FLAG tag in the cytoplasmic domain showed the same distribution as endogenous Aka protein and rescued *aka* mutants (Figure S2L-O). In sagittal sections of the epidermis, Aka was strongly enriched at junctions between three adjoining cells (Figure 3C). Aka was also detectable at BCJs, with on average 18-fold lower levels compared to TCJs (Figure S2A-B, N). At TCJs, Aka overlapped with the SJ protein Discs Large (Dlg; Woods and Bryant, 1991) along the apico-lateral membrane domain (Figure 3H, I), and localized just basally to adherens junctions marked by beta-Catenin/Armadillo (Arm; Figure 3E-G). In embryos homozygous for *aka* missense mutations (aka^{K104}, aka^{K93}, aka^{J55}, aka^{L224}), Aka was distributed inside cells (Figure 3D and data not shown), suggesting that the mutant Aka proteins are retained intracellularly or are internalized from the plasma membrane.

We compared the distribution of Aka and Gli using a Gli-YFP protein trap or anti-Gli antisera. We found that Aka and Gli co-localize at TCJs, both in ectoderm-derived epithelia that exhibit pleated SJs (Figure 3K, L, Figure S2C-I) and in the endodermal midgut that develops smooth SJs involving a different set of SJ proteins (Figure 3J, Figure S2K; Izumi et al., 2012), as well as in the extra-

embryonic amnioserosa (Figure S2J). The presence of Aka and Gli at TCJs in ectodermal and endodermal epithelia suggests that the two proteins are common components of TCJs.

aka is required for the formation of tricellular, but not bicellular junctions

Since the *aka* phenotype resembled mutants in SJ components, we asked whether SJ proteins were mislocalized in *aka* mutants. Fasciclin 3 (Fas3; Snow et al., 1989) concentrates at SJs without being required for viability (Whitlock, 1993), and becomes evenly distributed along lateral membranes in mutants with an impaired paracellular barrier (Behr et al., 2003; Paul et al., 2003; Wu et al., 2004). Fas3 was indeed mislocalized in epithelia of *aka* embryos (Figure 4A, B). By contrast, the claudin-like protein Sinuous (Sinu; Figure 4A, B; Wu et al., 2004), the Na pump α-subunit (Atpα Figure 4C, D; Paul et al., 2003), and the ERM protein Coracle (Cora; Figure 4E, F; Lamb et al., 1998), all of which are SJ core complex components (Oshima and Fehon, 2011), remained concentrated at apico-lateral membranes in *aka* mutants. Similarly, apico-lateral accumulation of the SJ-associated membrane proteins Lachesin (Lac)-YFP (Figure S3A, B; Llimargas et al., 2004) and Melanotransferrin (MTf; Tiklova et al., 2010; not shown) was not affected in *aka* mutants. The cytoplasmic polarity proteins Dlg, Scribble (Scrib; Bilder and Perrimon, 2000) and Lethal giant larvae (Lgl; Mechler et al., 1985) also localize to SJs, but are more mobile than the core complex (Oshima and Fehon, 2011). Dlg, Scrib, and Lgl were concentrated apico-laterally in *aka* mutants, similar to wild-type controls (Figure 4G-J and data not shown). All embryos were analyzed at early stage 16, when SJ components show apico-lateral localization and epithelia have developed functional paracellular barriers (Tepass and Hartenstein, 1994). The results therefore suggest that Aka is not required for assembly of bicellular SJs.

To address if recruitment of Aka to TCJs could depend on bicellular SJ formation, we analyzed Aka localization in *cora* embryos, in which SJs are severely reduced or absent (Lamb et al., 1998). Aka accumulated at TCJs in *cora* mutants with similar intensity as in controls, and retained its apico-lateral localization, unlike Fas3, which distributed along the entire lateral membrane (Figure 4K-N). Aka also accumulated at TCJs in *Mcr*, *Nrg* and *sinu* mutants, which lack SJs (Figure S3C-F; Genova and Fehon, 2003; Wu et al., 2004; Batz et al., 2014). Thus, Aka appears to localize to TCJs by a mechanism that is independent of bicellular SJ formation.

We next analyzed junction integrity in *aka* mutants by transmission EM. Lack of individual SJ components is associated with reduced or absent electron-dense septa (Lamb et al., 1998; Behr et al., 2003; Wu et al., 2004; Furuse and Tsukita, 2006). In stage 16 *aka* embryos, SJ septa spanning the space between two neighboring cells were present in the BCJ region (Figure 4O, P), although SJs appeared to disintegrate in later (stage 17) embryos, possibly as a consequence of defects in cell adhesion or epithelial barrier formation. We also analyzed TCJs, which are visible as bifurcations of the BCJs. In wild-type embryos, the dihedral angles of the three adjoining cell membranes were equal (120 degrees) around the bifurcation (Figure 4Q; Figure S4A-C; Graf et al., 1982). Three bicellular

limiting strands were described to delineate the TCJ space that contains a row of stacked diaphragms appearing as electron-dense material (Graf et al., 1982). In *aka* embryos, bicellular septa were present near TCJs, but the central TCJ space always lacked electron-dense material and the dihedral angles of the converging membranes were frequently unequal (Figure 4R). Consistent with these observations in *aka* embryos, RNAi-mediated depletion of Aka from wing imaginal disc cells led to a broader distribution of TCJ angles compared to control cells (Figure S4D-L). Together, these findings suggest that Aka is required specifically for the formation and correct geometry of TCJs, whereas bicellular SJ assembly is independent of *aka* function.

Aka is necessary and sufficient for accumulation of Gliotactin at tricellular junctions

To address Aka's role in TCJ formation, we asked whether Aka and Gli depend on each other for their ability to accumulate at TCJs. Whereas Aka and Gli co-localized at TCJs in the wild type (Figure 5A), TCJ accumulation of Gli was lost in *aka* mutant epithelia (Figure 5C). Instead, Gli was uniformly distributed around the cell circumference (Figure 5C'), although it remained enriched at the apico-lateral SJ domain (Figure S5C, D). By contrast, Aka still accumulated at TCJs in *Gli* mutants (Figure 5B). We also analyzed the distribution of Gli-YFP in larvae, in which we depleted Aka from stripes of cells by RNAi (Figure S5A, B). In control epidermal and wing imaginal disc cells, Gli-YFP accumulated at TCJs and was present at low levels at BCJs. In adjacent cells expressing *aka* dsRNA, Gli-YFP accumulation at TCJs was lost, whereas Gli-YFP signals at BCJs increased, consistent with re-distribution of Gli-YFP from TCJs to BCJs upon depletion of Aka. These findings suggest that Aka acts upstream of Gli in TCJ assembly.

In wild-type embryos, Gli is initially distributed throughout lateral membranes and begins to accumulate at TCJs during late stage 13 (Schulte et al., 2003). Strikingly, mis-expressing Aka in epidermal stripes before the onset of endogenous *aka* expression was sufficient to initiate premature TCJ accumulation of Gli at early stage 13 (Figure 5D), indicating that Aka is limiting for TCJ localization of Gli. However, Gal4-driven overexpression led to accumulation of Aka outside of TCJs, but was not able to direct Gli to ectopic locations. Thus, Aka appears to associate with Gli only in the context of TCJs. Together, these results suggest that Aka acts early in TCJ assembly by recruiting or maintaining Gli at tricellular vertices.

Aka's PDZ-binding motif is not required for maintaining Aka and Gli localization at TCJs

To understand how Aka localizes to tricellular vertices, we investigated the contributions of Aka's extracellular and cytoplasmic parts to TCJ localization. We used Tobacco Etch Virus (Tev) protease to release the Aka C-terminus including the PDZ-binding motif by cleaving the Aka-Ty1-Tev-SGFP-FLAG protein between the Ty1 and SGFP tags (Figure 6A). Membrane-tethered Tev protease was expressed in epidermal stripes of *aka* embryos carrying Aka-Ty1-Tev-SGFP-FLAG as the only source of Aka protein (Figure 6B). In Tev-expressing cells, the C-terminal fragment carrying the SGFP tag

became diffusely localized or degraded, whereas in the same cells the N-terminal fragment with the Ty1 tag remained localized at TCJs (Figure 6B, C). Similarly, TCJ accumulation of Gli remained unchanged upon Tev-mediated release of the Aka C-terminus (Figure 6D). However, we cannot rule out that incomplete Tev protease cleavage might leave an undigested fraction of Aka-Ty1-Tev-SGFP-FLAG protein that could support TCJ formation. We therefore generated a mutant Aka version lacking the PDZ-binding motif (UAS-Aka-ΔPDZB) and tested its function in *aka* embryos. Strikingly, Aka-ΔPDZB rescued tracheal defects (Figure 1E) and accumulation of Gli at TCJs in salivary glands (Figure 6H-J), although Fas3 was still mislocalized (Figure 6E-G). Together, these results indicate that Aka's C-terminus, including the PDZ-binding motif, is not required to maintain TCJ localization of Aka's extracellular part and of Gli.

The absence in the C-terminal part of conserved stretches other than the PDZ-binding motif suggested that Aka may be targeted to TCJs by cues outside the cytoplasmic domain. To test whether extracellular interactions between Aka proteins residing on adjacent cells could be involved in TCJ localization, we analyzed the distribution of Aka and Gli in mosaic situations where Aka was depleted from one or two cells abutting a three-cell vertex by RNAi (Figure 5E, Figure S5B). Interestingly, TCJ accumulation of Aka and Gli depends on Aka expression in all three adjoining cells, since Aka and Gli failed to accumulate at TCJs in situations where Aka was depleted from one or two of the cells (Figure 5F-F''', Figure S5B). This finding suggests that the extracellular domains of Aka molecules produced by different cells interact with each other. Consistent with this idea, S2 cells transfected with an Aka-mCherry construct formed aggregates (Figure 5G-J). Although we were not able to detect enrichment of Aka-mCherry at tricellular contacts in S2 cell aggregates, possibly due to the high expression levels upon transfection, these results indicate that Aka can mediate homophilic adhesion.

To explore if the geometry of tricellular vertices may theoretically suffice as cue to promote TCJ localization of Aka via extracellular interactions, we performed computer simulations. At TCJs, Aka molecules from different cells might form complexes, and such complexes are automatically contained to one instead of two dimensions (Figure 7C). A reduction of dimensionality can lead to increased binding rates (Adam and Delbrück, 1968; Richter and Eigen, 1974). Simulating this effect revealed a 40-fold enrichment of Aka at TCJs compared to BCJs after 2-2.5 h of simulated time (Figure 7D, Figure S1, Movie S1). However, this equilibrium was sensitive to parameter changes (see Supplemental Information). Thus, enrichment through self-assembly at TCJs may in principle emerge from the geometry of tricellular vertices combined with the capacity of a protein to multimerize, although additional factors are likely to be involved. Together, our findings suggest that TCJ localization results from the geometry of three-cell vertices and from Aka's intrinsic protein features, rather than from a TCJ-directed intracellular transport pathway.

Discussion

Ultrastructural analyses revealed a unique junctional architecture at points in epithelia where three cells meet. Yet, only few TCJ-specific proteins are known, and how they assemble into a tightly localized complex exclusively at tricellular vertices is not understood. Here we describe a transmembrane protein that plays a critical role in TCJ assembly and epithelial barrier formation. First, we show that Aka localizes to TCJs in ectodermal and endodermal epithelia, suggesting that Aka is a core TCJ component. Second, we demonstrate that Aka is specifically required for the assembly and correct geometry of tricellular, but not of bicellular SJs, and that Aka localizes to TCJs independently of bicellular SJs. Third, Aka is required for recruiting or maintaining Gli, the only other invertebrate TCJ component characterized so far, at tricellular vertices. Conversely, Gli is not required for TCJ localization of Aka. Fourth, Aka mis-expression causes premature accumulation of Gli at TCJs, indicating that Aka acts upstream of Gli in initiating TCJ formation.

Aka protein contains a large extracellular domain with a conserved tripartite repeat structure. This unique structure distinguishes Aka from other known TCJ proteins. Tricellulin, a four-pass transmembrane protein in vertebrates, localizes to the central sealing elements, suggesting that it participates in the specialized bicellular contacts that surround each three-cell vertex (Ikenouchi et al., 2005). Tricellulin is recruited to TCJs by the immunoglobulin domain transmembrane protein LSR, but how LSR localizes to TCJs is still unclear (Masuda et al., 2011). In *Drosophila,* Gli, a transmembrane protein with a cholinesterase domain lacking catalytic activity, accumulates at TCJs, but is also involved in bicellular SJ organization (Genova and Fehon, 2003; Schulte et al., 2003). Phosphorylation-dependent endocytic turnover and indirect association with Dlg are required for accumulation of Gli at TCJs (Schulte et al., 2006; Padash-Barmchi et al., 2010; Padash-Barmchi et al., 2013). However, the mechanisms underlying TCJ-specific localization are not understood for Gli or any other TCJ protein.

Our results suggest that Aka acts at an early step during TCJ assembly by recruiting other TCJ components, including Gli, to tricellular vertices. TCJ localization of Aka and Gli does not require Aka's C-terminus, including the PDZ-binding motif. Similarly, Gli was found to localize to TCJs independently of its PDZ-binding motif (Schulte et al., 2006). These findings suggest that Aka and Gli might be targeted to TCJs through their extracellular domains, rather than through a cytoplasmic localization machinery. Since mislocalized Aka protein is not sufficient to recruit Gli to ectopic locations, Aka might not interact directly with Gli, or only do so in the context of TCJs. Consistent with this notion, we were not able to detect co-immunoprecipitation of Aka and Gli (not shown). Interestingly, overexpression of Gli (Schulte et al., 2006) or absence of Aka causes Gli to spread from TCJs to BCJs. Thus, Gli does not have an intrinsic propensity to localize to TCJs, but by default localizes to the apicolateral membrane domain occupied by SJs along the cell perimeter. TCJ accumulation of Gli therefore requires (i) association with the apicolateral membrane and, (ii) Aka-dependent recruitment of Gli specifically to TCJs. Our findings show that unlike Gli, Aka does not

depend on bicellular SJs for its localization to TCJs, and suggest that Aka protein might have intrinsic properties that lead to its accumulation at TCJs.

Tricellular vertices display a unique geometry where three plasma membranes are in close proximity and at fixed angles (Figure 7A, B). The exceptional curvature of the plasma membrane at these sites implies distinct physical properties compared to bicellular contacts. Intriguingly, we found that TCJ assembly depends on Aka expression in all three cells adjoining a vertex, suggesting that extracellular interactions between Aka molecules from different cells are essential for TCJ formation. Considering the size of Aka's extracellular domain (303 kDa), it is likely that a single Aka protein spans the entire TCJ canal (25-30 nm; Graf et al., 1982; Noirot-Timothee et al., 1982), although shorter Aka isoforms may constitute different structures. Shorter Aka species might carry out functions that may or may not be related to the function of full-length Aka at TCJs. Alternatively, Aka fragments may reflect turnover of TCJ complexes, *e.g*., during junctional remodeling.

It is tempting to speculate that the three repeat regions in full-length Aka protein, with apparent similar domain organization, could make equal contacts with the three cell corners in the plane perpendicular to the central TCJ canal. Possibly, interaction with membrane components in the tricellular region occurs via the three SR domains, since such domains are found in receptors that recognize a wide range of molecular patterns, including surface proteins, carbohydrates, lipids, lipopolysaccharides, and peptidoglycans associated with pathogens or apoptotic cells (Bowdish and Gordon, 2009). As such three-way contacts may, for steric reasons, only be possible at vertices, they might selectively stabilize Aka complexes at these sites. Our computer simulations suggest that the enrichment of Aka at three-cell vertices could theoretically be enhanced by the reduction of dimensionality in the tricellular region, which may promote stacking interactions between Aka molecules within the central TCJ canal. This idea is consistent with the regular structure of the TCJ diaphragms and the equal dihedral angles near TCJs as observed by EM (Fristrom, 1982; Graf et al., 1982; Noirot-Timothee et al., 1982). Stacking might occur with Aka molecules rotated by 120 or 240 degrees within the stack, perhaps in a helical array, depending on the contributing cell (Figure S6 H). Notably, such a scenario would explain our finding that TCJ formation requires Aka protein production by all three cells adjoining a vertex. A high priority of future studies will be to investigate the arrangement of Aka proteins at TCJs. Together, our results on Aka localization, the geometry of three-cell vertices, and the triple-repeat structure of Aka protein suggest a mechanism of TCJ formation, which is promoted by self-assembly of Aka at tricellular contacts. Such self-assembly might additionally involve interactions with other membrane-associated or extracellular components, and could cooperate with bicellular adhesion molecules that zip up bicellular contacts. It will be interesting to test whether the geometry of tricellular vertices and the specific properties of Aka protein are sufficient to direct its accumulation to TCJs. Conversely, perturbed TCJ geometry upon loss of Aka may have long-range effects, such as the loss of cell-cell adhesion that we observed in late-stage *aka* embryos. Interestingly, depletion of

Tricellulin from mammalian cells affects cell shape and the F-actin network, suggesting that TCJs may in fact have organizing activity on the entire cell (Oda et al., 2014).

The existence of *aka* homologues in invertebrates and cephalochordates correlates with the presence of SJs in these groups (Banerjee et al., 2006). However, the proposed self-assembly model for TCJ formation in *Drosophila* may apply also to vertebrates, although the corresponding proteins remain to be discovered. A better understanding of TCJ assembly will be a key step towards elucidating how these poorly characterized cellular structures provide epithelial barrier function, while at the same time allowing the passage of migrating lymphocytes, metastatic cells, and intracellular pathogens.

Experimental Procedures

Genetics

Fly stocks are described in FlyBase unless mentioned otherwise: aka^{YD1046} (Quinones-Coello et al., 2007), *Df(2L)Exel6009*, *Df(2L)BSC171*, *CyO Dfd-YFP*, *btl-Gal4*, *en-Gal4*, *hh-Gal4*, *69B-Gal4*, *UAS-mCherry-nls*, *UAS-Verm-mRFP*, *UAS-α-Catenin-GFP*, *DE-Cad-mTomato*, *UAS-TevP-P* (prenylated Tev protease; gift from Marko Brankatschk, Dresden, Germany), $cora^{1}$, Mcr^{K103}, Nrg^{I7}, $sinu^{06524}$, $UAS\text{-}lacZ^{RNAi}$, *UAS-dicer2* (VDRC-60014), *Dlg-GFP* (YC0005), *Scrib-GFP* (CA07683), *Nrx-IV-GFP* (CA06597; Quinones-Coello et al., 2007), *Gli-YFP* (CPTI-002805), *Lac-YFP* (CPTI-002601), *Nrg-YFP* (CPTI-001714; Lowe et al., 2014). For tracheal-specific RNAi, $UAS\text{-}aka^{RNAi}$ (VDRC-52608) and *UAS-dicer2* were co-expressed using *btl-Gal4*. *aka* and *Gli* mutations were induced by ethylmethanesulfonate (EMS) mutagenesis (see Supplemental Information). *Gli* alleles were Gli^{dv3} (Schulte et al., 2003), $Gli^{AE2delta45}$ (Auld et al., 1995), Gli^{F156} and Gli^{F176} (this work). Gli^{F156} has a deletion of a single nucleotide (C3893), resulting in a frame shift and a premature stop codon after 476 aa within the Cholinesterase domain. Gli^{F176} has a C4901>T transition, resulting in a premature stop codon after 724 aa within the transmembrane domain.

Antibodies and immunostainings

Embryos were fixed in 4% formaldehyde in PBS/heptane for 20 min and devitellinized by shaking in methanol/heptane. Embryos for anti-Aka immunostainings were heat-fixed. Antibodies were chicken anti-GFP (1:500, Abcam), mouse anti-GFP (1:300; Clontech), mouse anti-Cora (1:20; Lamb et al., 1998), mouse anti-Gli 1F6 (1:200; Auld et al., 1995), mouse anti-Dlg 4F3 (1:500; DSHB), mouse anti-Fas3 7G10 (1:50; DSHB), mouse anti-TY1 BB2 (1:500; Sigma), mouse anti-Arm N27A1 (1:7, DSHB), rat anti-HA 3F10 (1:300; Roche), rabbit anti-Lgl (1:200; Santa Cruz), rabbit anti-Sinu (1:500; Wu et al., 2004), guinea pig anti-Mtf (1:500; Tiklova et al., 2010). Goat secondary antibodies were conjugated with Alexa 405, Alexa 488, Alexa 568 (Molecular Probes), or Cy5 (Jackson ImmunoResearch). Chitin was detected using AlexaFluor-SNAP-tagged chitin-binding domain from *Bacillus circulans* chitinase A1 prepared as described (Caviglia and Luschnig, 2013). The anti-Aka

antiserum was generated by GenScript (NJ, USA) by immunizing rabbits with the peptide CRTEGGTPAGRRGQP (corresponding to aa 2933-2946 in Aka-PB). The antiserum was affinity-purified and used at a dilution of 1:500 for immunostainings.

Immunoblotting

Lysates were prepared by homogenizing 200 embryos (stage 14-16) in 100 µl sample buffer (Invitrogen). Extracts were heated at 70°C for 5 min before loading on Novex NuPAGE™ 4-12% Bis-Tris gels (Life Technologies) and blotting onto PVDF membranes (Pore size 0.2 µm, Millipore). Primary antibodies (rabbit anti-Aka (1:10,000), mouse anti-α-tubulin (1:10,000; Sigma)) were detected with HRP-conjugated secondary antibodies (1:2,500; Cell Signaling) and ECL+ (Pierce).

Dextran Injections

Rhodamine-labeled dextran (10 kDa; Molecular Probes) was injected as described (Lamb et al., 1998) into wild-type and *aka*^{L200} embryos carrying *btl-Gal4 UAS-GFP* to label tracheal cells. Embryos were imaged 20 minutes after injection.

Cell aggregation assay

Drosophila S2 cells were cultured in Schneider's medium (Invitrogen) at 27°C. Cells were transfected with pUASTattB-Aka-mCherry, pUAST-Nrg167-GFP (positive control; D. Siegenthaler, E. Moreno and J. Pielage, unpublished), or pUbi-nlsGFP (negative control). pCaSpeR4-Act5c-GAL4 was co-transfected to drive expression of UAS constructs. 800,000 cells were transfected with 1 µg plasmid DNA using FuGene HD transfection reagent (Invitrogen). After three days, cells were dissociated by repeated pipetting. Density was adjusted to $1*10^6$ cells/ml with Schneider's medium. 0.5 ml cell suspension was shaken for 2.5 hours at 100 rpm in an Eppendorf tube at room temperature. To analyze aggregation, cells were spotted on a slide and observed using epifluorescence/DIC. The number of transfected (GFP- or mCherry-positive) single cells and cells in clusters (containing at least 3 cells) was determined by manual counting. Transfections were performed in duplicate.

Author contributions

All authors designed and conducted experiments and analysed the data. T.A.W. performed computer simulations and wrote corresponding sections of the text. A.U. and S.L. wrote the manuscript.

Acknowledgements

We are indebted to Kristina Armbruster and Stefanie Limmer, who isolated the *aka* mutants. We thank Markus Affolter, Vanessa Auld, Marko Brankatschk, Rick Fehon, Jan Pielage, Frank Schnorrer, Pavel Tomancak, the Bloomington and Kyoto *Drosophila* stock centers, the Vienna *Drosophila* Resource Center, and the Developmental Studies Hybridoma Bank for providing fly stocks and reagents. The Centre for Cellular Imaging and the Proteomics Core Facility, both at GU, provided support with confocal imaging and protein identification. The electron microscopy unit at GU and the Center for Microscopy and Image Analysis at UZH provided support with electron microscopy. We thank Dominique Förster and Martina Trost for help with experiments, Mark Robinson and Benjamin Risse for advice on statistics, Riccardo Murri and Antonio Messina (Grid Computing Competence Center, UZH) for computer support, and Daniel Wechsler, Tobias Grubenmann, Prasenjit Saha and Christof Aegerter for discussions. S.L. would like to thank Christian Lehner for continuous support and discussions. JG was supported by a Forschungskredit fellowship of the UZH. Work in AU's laboratory was supported by the Swedish Cancer Society and the University of Gothenburg. Work in SL's laboratory was supported by the Swiss National Science Foundation (SNF ProDoc_PDFMP3_127362, SNF 31003A_141093_1), the University of Zürich, and the Kanton Zürich.

References

Adam, G., and Delbrück, M. (1968). Reduction of Dimensionality in Biological Diffusion Processes. In Structural Chemistry and Molecular Biology, A. Rich, and N. Davidson, eds. (San Francisco, W H Freeman and Co.).

Auld, V.J., Fetter, R.D., Broadie, K., and Goodman, C.S. (1995). Gliotactin, a novel transmembrane protein on peripheral glia, is required to form the blood-nerve barrier in Drosophila. Cell *81*, 757-767.

Banerjee, S., Bainton, R.J., Mayer, N., Beckstead, R., and Bhat, M.A. (2008). Septate junctions are required for ommatidial integrity and blood-eye barrier function in Drosophila. Developmental Biology *317*, 585-599.

Banerjee, S., Sousa, A.D., and Bhat, M.A. (2006). Organization and function of septate junctions: an evolutionary perspective. Cell Biochem Biophys *46*, 65-77.

Batz, T., Forster, D., and Luschnig, S. (2014). The transmembrane protein Macroglobulin complement-related is essential for septate junction formation and epithelial barrier function in Drosophila. Development *141*, 899-908.

Behr, M., Riedel, D., and Schuh, R. (2003). The claudin-like megatrachea is essential in septate junctions for the epithelial barrier function in Drosophila. Developmental Cell *5*, 611-620.

Bilder, D., and Perrimon, N. (2000). Localization of apical epithelial determinants by the basolateral PDZ protein Scribble. Nature *403*, 676-680.

Bowdish, D.M., and Gordon, S. (2009). Conserved domains of the class A scavenger receptors: evolution and function. Immunol Rev *227*, 19-31.

Burns, A.R., Walker, D.C., Brown, E.S., Thurmon, L.T., Bowden, R.A., Keese, C.R., Simon, S.I., Entman, M.L., and Smith, C.W. (1997). Neutrophil transendothelial migration is independent of tight junctions and occurs preferentially at tricellular corners. Journal of Immunology *159*, 2893-2903.

Caviglia, S., and Luschnig, S. (2013). The ETS domain transcriptional repressor Anterior open inhibits MAP kinase and Wingless signaling to couple tracheal cell fate with branch identity. Development *140*, 1240-1249.

Chakraborty, P., William Buaas, F., Sharma, M., Smith, B.E., Greenlee, A.R., Eacker, S.M., and Braun, R.E. (2014). Androgen-dependent sertoli cell tight junction remodeling is mediated by multiple tight junction components. Mol Endocrinol *28*, 1055-1072.

Forster, D., Armbruster, K., and Luschnig, S. (2010). Sec24-dependent secretion drives cell-autonomous expansion of tracheal tubes in Drosophila. Current Biology *20*, 62-68.

Fristrom, D.K. (1982). Septate junctions in imaginal disks of Drosophila: a model for the redistribution of septa during cell rearrangement. The Journal of Cell Biology *94*, 77-87.

Fukumatsu, M., Ogawa, M., Arakawa, S., Suzuki, M., Nakayama, K., Shimizu, S., Kim, M., Mimuro, H., and Sasakawa, C. (2012). Shigella targets epithelial tricellular junctions and uses a noncanonical clathrin-dependent endocytic pathway to spread between cells. Cell Host & Microbe *11*, 325-336.

Furuse, M., Izumi, Y., Oda, Y., Higashi, T., and Iwamoto, N. (2014). Molecular organization of tricellular tight junctions. Tissue Barriers *2*, e28960.

Furuse, M., and Tsukita, S. (2006). Claudins in occluding junctions of humans and flies. Trends in Cell Biology *16*, 181-188.

Genova, J.L., and Fehon, R.G. (2003). Neuroglian, Gliotactin, and the Na+/K+ ATPase are essential for septate junction function in Drosophila. The Journal of Cell Biology *161*, 979-989.

Graf, F., Noirot-Timothee, C., and Noirot, C. (1982). The specialization of septate junctions in regions of tricellular junctions. I. Smooth septate junctions (=continuous junctions). J Ultrastruct Res *78*, 136-151.

Higashi, T., Tokuda, S., Kitajiri, S., Masuda, S., Nakamura, H., Oda, Y., and Furuse, M. (2013). Analysis of the 'angulin' proteins LSR, ILDR1 and ILDR2--tricellulin recruitment, epithelial barrier function and implication in deafness pathogenesis. Journal of Cell Science *126*, 966-977.

Ikenouchi, J., Furuse, M., Furuse, K., Sasaki, H., and Tsukita, S. (2005). Tricellulin constitutes a novel barrier at tricellular contacts of epithelial cells. The Journal of Cell Biology *171*, 939-945.

Izumi, Y., Yanagihashi, Y., and Furuse, M. (2012). A novel protein complex, Mesh-Ssk, is required for septate junction formation in the Drosophila midgut. Journal of Cell Science *125*, 4923-4933.

Jaspers, M.H., Nolde, K., Behr, M., Joo, S.H., Plessmann, U., Nikolov, M., Urlaub, H., and Schuh, R. (2012). The claudin Megatrachea protein complex. The Journal of Biological Chemistry *287*, 36756-36765.

Kelley, L.A., and Sternberg, M.J. (2009). Protein structure prediction on the Web: a case study using the Phyre server. Nat Protoc *4*, 363-371.

Krug, S.M., Amasheh, S., Richter, J.F., Milatz, S., Gunzel, D., Westphal, J.K., Huber, O., Schulzke, J.D., and Fromm, M. (2009). Tricellulin forms a barrier to macromolecules in tricellular tight junctions without affecting ion permeability. Molecular Biology of the Cell *20*, 3713-3724.

Lamb, R.S., Ward, R.E., Schweizer, L., and Fehon, R.G. (1998). Drosophila coracle, a member of the protein 4.1 superfamily, has essential structural functions in the septate junctions and developmental functions in embryonic and adult epithelial cells. Mol Biol Cell *9*, 3505-3519.

Llimargas, M., Strigini, M., Katidou, M., Karagogeos, D., and Casanova, J. (2004). Lachesin is a component of a septate junction-based mechanism that controls tube size and epithelial integrity in the Drosophila tracheal system. Development *131*, 181-190.

Lowe, N., Rees, J.S., Roote, J., Ryder, E., Armean, I.M., Johnson, G., Drummond, E., Spriggs, H., Drummond, J., Magbanua, J.P., *et al.* (2014). Analysis of the expression patterns, subcellular localisations and interaction partners of Drosophila proteins using a pigP protein trap library. Development *141*, 3994-4005.

Masuda, S., Oda, Y., Sasaki, H., Ikenouchi, J., Higashi, T., Akashi, M., Nishi, E., and Furuse, M. (2011). LSR defines cell corners for tricellular tight junction formation in epithelial cells. Journal of Cell Science *124*, 548-555.

Mechler, B.M., McGinnis, W., and Gehring, W.J. (1985). Molecular cloning of lethal(2)giant larvae, a recessive oncogene of Drosophila melanogaster. The EMBO journal *4*, 1551-1557.

Nakai, K., Tanaka, T., Murai, T., Ohguro, N., Tano, Y., and Miyasaka, M. (2005). Invasive human pancreatic carcinoma cells adhere to endothelial tri-cellular corners and increase endothelial permeability. Cancer Science *96*, 766-773.

Noirot-Timothee, C., Graf, F., and Noirot, C. (1982). The specialization of septate junctions in regions of tricellular junctions. II. Pleated septate junctions. J Ultrastruct Res *78*, 152-165.

Noirot-Timothee, C., and Noirot, C. (1980). Septate and scalariform junctions in arthropods. Int Rev Cytol *63*, 97-140.

Oda, Y., Otani, T., Ikenouchi, J., and Furuse, M. (2014). Tricellulin regulates junctional tension of epithelial cells at tricellular contacts via Cdc42. Journal of Cell Science, *in press.*

Oshima, K., and Fehon, R.G. (2011). Analysis of protein dynamics within the septate junction reveals a highly stable core protein complex that does not include the basolateral polarity protein Discs large. Journal of Cell Science *124*, 2861-2871.

Padash-Barmchi, M., Browne, K., Sturgeon, K., Jusiak, B., and Auld, V.J. (2010). Control of Gliotactin localization and levels by tyrosine phosphorylation and endocytosis is necessary for survival of polarized epithelia. Journal of Cell Science *123*, 4052-4062.

Padash-Barmchi, M., Charish, K., Que, J., and Auld, V.J. (2013). Gliotactin and Discs large are co-regulated to maintain epithelial integrity. Journal of Cell Science *126*, 1134-1143.

Paul, S., Ternet, M., Salvaterra, P.M., and Beitel, G. (2003). The Na+/K+ ATPase is required for septate junction function and epithelial tube-size control in the Drosophila tracheal system. Development *130*, 4963-4974.

Quinones-Coello, A.T., Petrella, L.N., Ayers, K., Melillo, A., Mazzalupo, S., Hudson, A.M., Wang, S., Castiblanco, C., Buszczak, M., Hoskins, R.A.*, et al.* (2007). Exploring strategies for protein trapping in Drosophila. Genetics *175*, 1089-1104.

Riazuddin, S., Ahmed, Z.M., Fanning, A.S., Lagziel, A., Kitajiri, S., Ramzan, K., Khan, S.N., Chattaraj, P., Friedman, P.L., Anderson, J.M.*, et al.* (2006). Tricellulin is a tight-junction protein necessary for hearing. American journal of human genetics *79*, 1040-1051.

Richter, P.H., and Eigen, M. (1974). Diffusion controlled reaction rates in spheroidal geometry. Application to repressor—operator association and membrane bound enzymes. . Biophys Chem *2*, 255-263.

Schulte, J., Charish, K., Que, J., Ravn, S., MacKinnon, C., and Auld, V.J. (2006). Gliotactin and Discs large form a protein complex at the tricellular junction of polarized epithelial cells in Drosophila. Journal of Cell Science *119*, 4391-4401.

Schulte, J., Tepass, U., and Auld, V.J. (2003). Gliotactin, a novel marker of tricellular junctions, is necessary for septate junction development in Drosophila. The Journal of Cell Biology *161*, 991-1000.

Schultz, J., Milpetz, F., Bork, P., and Ponting, C.P. (1998). SMART, a simple modular architecture research tool: identification of signaling domains. Proceedings of the National Academy of Sciences of the United States of America *95*, 5857-5864.

Snow, P.M., Bieber, A.J., and Goodman, C.S. (1989). Fasciclin III: a novel homophilic adhesion molecule in Drosophila. Cell *59*, 313-323.

Staehelin, L.A. (1973). Further observations on the fine structure of freeze-cleaved tight junctions. Journal of Cell Science *13*, 763-786.

Tepass, U., and Hartenstein, V. (1994). The development of cellular junctions in the Drosophila embryo. Developmental Biology *161*, 563-596.

Tiklova, K., Senti, K.A., Wang, S., Graslund, A., and Samakovlis, C. (2010). Epithelial septate junction assembly relies on melanotransferrin iron binding and endocytosis in Drosophila. Nature Cell Biology *12*, 1071-1077.

Whitlock, K.E. (1993). Development of Drosophila wing sensory neurons in mutants with missing or modified cell surface molecules. Development *117*, 1251-1260.

Woods, D.F., and Bryant, P.J. (1991). The discs-large tumor suppressor gene of Drosophila encodes a guanylate kinase homolog localized at septate junctions. Cell *66*, 451-464.

Wu, V.M., Schulte, J., Hirschi, A., Tepass, U., and Beitel, G. (2004). Sinuous is a Drosophila claudin required for septate junction organization and epithelial tube size control. The Journal of Cell Biology *164*, 313-323.

Figure Legends

Figure 1

***aka* is required for tracheal tube size control and epithelial barrier formation.**

(A-E) Living stage 16 embryos expressing cytoplasmic GFP (green) and secreted Verm-RFP (magenta) in tracheal cells. *aka* mutants (B) and embryos expressing *UAS-aka*^{RNAi} in tracheal cells under the control of *btl*-Gal4 (C) show over-elongated tracheal tubes with reduced levels of luminal Verm-RFP, compared to the wild type (A). The tracheal defects of *aka* embryos are rescued by tracheal specific expression of wild-type Aka (*UAS-aka*; D) or of an Aka variant lacking the C-terminal PDZ-binding motif (*UAS-akaΔPDZB*; E). Right-hand panels (A''-E'') show close-up views of boxed regions in (A'-E').

(F, G) Embryos expressing cytoplasmic GFP (green) in tracheal cells were injected with fluorescent 10 kDa dextran (magenta) at stage 16. Dextran is largely excluded from the tracheal lumen of wild-type embryos (F), but rapidly enters the lumen in *aka* mutants (G).

(H, I) Close-ups of tracheal transverse connective in living wild-type (H) and *aka* embryos (I) expressing cytoplasmic GFP. Note the cavities devoid of GFP in the *aka* mutant epithelium.

(J-K'') TEM sections of wild-type (J) and *aka* mutant (K) epidermis with schematic drawings (J', K') to indicate plasma membranes and nuclei ("n"). Each cavity in (K) is flanked by two BCJs, indicating

that cavities form between two cells. (K'') shows higher magnification of the region marked by a box in (K'). Arrowheads point to two BCJs flanking a cavity.

Scale bars: 50 µm (A-E); 10 µm (A''-E''); 20 µm (F, G); 5 µm (H, I); 2 µm (J, K); 2 µm (K'').

Figure 2

***aka* encodes a large transmembrane protein with a tripartite extracellular domain.**

(A) Genomic organization of the *aka* locus. Exons are shown as boxes with coding regions in black.

(B) Domain organization of Aka protein. The signal peptide (SP), extracellular domain (2716 aa), transmembrane domain (TM), and cytoplasmic tail (384 aa) with the PDZ-binding motif (ETAM) are indicated. SMART predicts three scavenger receptor cysteine-rich domains (SR), a CUB domain, a C-type lectin domain (CLECT), and nineteen parallel beta-helix repeats (blue) in the extracellular part. Mutations in *aka* alleles are indicated. The anti-Aka antiserum was raised against a peptide in the cytoplasmic part (arrow). Asterisks indicate the positions of the six tryptic peptides detected for the C-terminal Aka cleavage product.

(C) Aka's extracellular domain exhibits a tripartite repeat structure. Phyre predicts an N-terminal SR domain, a central CUB-like domain and a C-terminal single-stranded right-handed beta helix in each repeat (colored boxes; 84-100% confidence). Hmmer indicates similarity in the N- and C-terminal regions between each repeat. Grey boxes show regions that align with the 816 aa profile-hmm. Conditional E-values are 0.0 for region I, 7.0e-34 and 1.9e-08 for region II, and 1.0e-37 and 9.5e-4 for region III. Arrowhead indicates the approximate Aka cleavage site.

(D, E) Immunoblot of embryonic extracts probed with anti-Aka. (D) Wild-type embryos produce full-length Aka above 250 kDa and two smaller Aka species around 150 kDa (arrowheads). Asterisks indicate non-specific bands also detected in *Df(2L)BSC171* ("Df") embryos. Specific Aka signals are absent from aka^{L200}, aka^{N43} and aka^{J210} embryos, whereas full-length Aka, but not the lower-MW species, are present in *aka* mis-sense alleles (aka^{J55}, aka^{L224}, aka^{K93}, aka^{K104}). (E) Incubation of extracts with N-glycanase causes a shift in Aka mobility (lanes 3 and 4), suggesting that Aka is N-glycosylated. Non-reducing conditions do not alter electrophoretic mobility (lanes 1 and 2).

(F-L) *In situ* hybridization shows *aka* expression in embryonic epithelia and CNS. Expression is first detected at stage 13 (F), increases in epidermis, tracheae, foregut and hindgut during stages 14 and 15 (G, H), and declines at late stage 15 (I; lateral views, dorsal up). CNS expression is detectable from stage 16 (J, K, ventral views). No transcripts were detected in *Df(2L)Exel6009* embryos (L).

Scale bars: 50 µm (F-I, L); 10 µm (J, K).

See also Figure S1.

Figure 3

Aka protein accumulates at tricellular junctions.

(A, B) Epifluorescence images of stage 16 embryos labeled with anti-Aka show Aka protein in the epidermis, tracheae and hindgut in the wild type (A), while only autofluorescent signals are seen in aka^{L200} embryos (B).

(C-G) Confocal sections of stage 16 embryos co-labeled with anti-Aka (magenta) and anti-Arm (green). Aka localization at TCJs is shown by *en face* view of wild-type epidermis (ep; C, C'). In aka^{K104} homozygotes, Aka is detected intracellularly (D, D'). Lateral views of hindgut (hg; E) and salivary gland (sg; F, G) epithelia reveal Aka localization just basal to adherens junctions labeled by Arm. No Aka staining is detected in aka^{L200} homozygotes shown here for salivary glands (G).

(H, I) Cross-sections of tracheal (tr; H-H'') and hindgut (I-I'') epithelia of wild-type embryos labeled with anti-Aka (magenta) and anti-Dlg (green) show overlapping distribution of Aka and Dlg along the apical-basal axis. Stippled line in (I) indicates the basal cell surface.

(J) Aka is detected at TCJs in the endodermal midgut (mg) epithelium (J-J''; *en face* view, Z-projection).

(K) *En face* view of hindgut epithelium of an embryo expressing Gli-YFP. Triple labeling for YFP (red), Aka (green) and Cora (blue) demonstrates co-localization of Aka and Gli at TCJs.

(L) Lateral view of hindgut epithelium in wild-type embryo labeled with anti-Aka (magenta) and anti-Gli (green) shows co-localization of the two proteins along the apical to basal axis of TCJs. Stippled line indicates the basal surface.

Scale bars: 50 µm (A, B); all other panels: 5 µm.

See also Figure S2.

Figure 4

Localization of Aka and of septate junction proteins are mutually independent.

(A, B) Wild-type and aka^{L200} embryos labeled for Fas3 (magenta) and Sinu (green). Fas3 and Sinu localize to the apical-most third of the lateral membrane in the hindgut epithelium (A-A''). In aka^{L200} mutants, Fas3 is mislocalized and distributes along the entire lateral cell surface, while Sinu retains its normal apico-lateral localization (B-B'').

(C-H) Wild-type and aka^{L200} embryos labeled for ATPα (C, D), Cora (E, F) or Dlg (G, H). The three SJ components show similar apico-lateral localization in the hindgut of wild-type (C, E, G) and *aka* (D, F, H) embryos.

(I, J) Images of living embryos show apico-lateral localization of Scrib-GFP in wild-type (I) and *aka* mutant (J) hindgut epithelium.

(K-N) Wild-type and *cora*^{1} embryos labeled for Aka (magenta) and Fas3 (green). Fas3 and Aka accumulate apico-laterally in wild-type hindgut (K-K''). In *cora* mutants, Aka localization is similar to that observed in the wild type, while Fas3 is detected along the entire lateral cell surface (L-L''). *En face* view shows that Aka localizes to TCJs in the wild-type (M, M') and *cora*^{1} mutant (N, N') hindgut. All embryos were at early stage 16.

(O-R) Transmission EM micrographs of epidermis in stage 16 (O, P; sectioned along apical-basal axis) and stage 17 (Q, R; sectioned parallel to apical surface) embryos. Note that bicellular SJ septa (red arrowheads) are present in wild-type (O, Q) and *aka*^{L200} (P, R) embryos. For Q and R, schematic drawings indicate the course of the plasma membrane. Small insets show close-ups of TCJs. Electron-dense material in the TCJ center is absent from TCJs in *aka* mutants. Also note that the dihedral angles of bicellular membranes are equal (120 degrees, indicated by red stars in bottom panels) close to the TCJ in the wild type, whereas angles are unequal in the *aka* mutant.

Scale bars: 5 µm (A-N); 200 nm (O, P); 250 nm (Q, R).

See also Figures S3 and S4.

Figure 5

Aka is necessary and sufficient for accumulation of Gliotactin at tricellular junctions and mediates adhesion in S2 cells.

(A-C) *En face* view of epidermis in stage 16 embryos labeled with Anti-Gli (magenta) and anti-Aka (green). Aka and Gli accumulate at TCJs in the wild type (A). Aka also accumulates at TCJs in *Gli* embryos, in which Gli is not detectable (B). In *aka* mutant embryos, Gli fails to accumulate at TCJs, but spreads along BCJs (C).

(D) *En face* view of epidermis in early stage 13 wild-type embryo labeled with Anti-Gli (magenta) and anti-Aka (green). Aka was expressed prematurely in epidermal stripes under the control of *en*-Gal4. Prior to the onset of endogenous Aka expression, Gli is distributed along BCJs. Note that in cells that express Aka prematurely Gli accumulates at TCJs.

(E) Stage 16 embryo expressing αCat-GFP (green) and *aka*^{RNAi} under the control of *en*-Gal4. Gli (red) fails to accumulate at TCJs in *aka*^{RNAi}-expressing stripes of cells, from which Aka (blue) is depleted.

(F-F''') Close-up of epidermis as in (E). Gli (F''', red in F) accumulates at TCJs in unperturbed control cells, whereas Gli distributes along BCJs in *aka*^{RNAi}-expressing cells marked by αCat-GFP. Aka (blue in F) is depleted from *aka*^{RNAi}-expressing cells (F''). Note that Aka and Gli accumulate at TCJs only when Aka expression in all three cells abutting a TCJ is unperturbed (blue circles in F'),

whereas Aka and Gli accumulation at TCJs is lost when Aka is depleted from one (green circles), two (red circles), or all three (white circles) cells adjoining a three-cell vertex.

(G-I') S2 cells were transfected with Aka-mCherry (magenta; G), Nrg167-GFP (green; H), or nlsGFP (green; I) constructs. Cells expressing Aka-mCherry or Nrg167-GFP, but not nlsGFP-expressing cells, form aggregates. (G-H) are bright-field images overlaid with epifluorescence images shown in (G'-I'). Insets show close-up views of cells marked by boxes in (G'-I'). Note that cell clusters in (G) consist of Aka-mCherry-expressing cells only and do not include non-transfected cells, suggesting that Aka mediates homophilic adhesion.

(J) Quantification of cell aggregation. Bars show the percentage of transfected cells (positive for GFP or mCherry, respectively) found in aggregates or as single cells, respectively. n=188 (Aka-mCherry); n=150 (Nrg167-GFP); n=400 (nls-GFP).

Scale bars: 10 µm (A-C, D); 50 µm (E); 5 µm (F-F'''); 100 µm (G-I').

See also Figure S5.

Figure 6

The Aka C-terminus is not required for maintaining TCJ localization of Aka's extracellular part and of Gliotactin.

(A) Structure of the Aka-Ty1-Tev-SGFP-FLAG construct. Positions of the 2xTy1 epitope tag, the Tev protease cleavage site (TEV), the superfolder GFP (SGFP) sequence, and the C-terminal PDZ-binding motif (PLETAM) are indicated (not drawn to scale with the rest of the protein).

(B) Confocal section of an embryo expressing Aka-Ty1-Tev-SGFP-FLAG as the only source of Aka protein. Prenylated Tev protease (UAS-TevP-P) is expressed in epidermal stripes under the control of *hh*-Gal4. N- and C-terminal portions of Aka were detected by anti-Ty1 and anti-GFP staining, respectively. Note that GFP staining is severely reduced in segmental stripes (B''), whereas Ty1 staining is unchanged along the embryo (B').

(C-D) Close-up views of embryonic epidermis as in (B) with Tev-expressing cells marked by co-expression of nls-mCherry. The C-terminal Aka fragment detected with anti-GFP becomes diffusely localized or degraded in Tev-expressing cells, whereas the Aka N-terminal fragment detected by anti-Ty1 staining (C''), as well as Gli (D''), remain localized at TCJs.

(E-J) Salivary glands from stage 16 embryos labeled for Fas3 (E-G) or Gli (H-J; *en face* view). 69B-Gal4 was used to drive expression of Aka (UAS-Aka; F) or of an Aka variant lacking the C-terminal PDZ-binding motif (UAS-AkaΔPDZB; G, J) in salivary glands. Fas3 localizes apico-laterally in wild-type (E) and in *aka* embryos expressing Aka (F), but is mislocalized along the entire lateral membrane in *aka* embryos expressing AkaΔPDZB (G). Gli localizes to TCJs in the wild type (H) and along BCJs

in *aka* embryos (I). Expression of AkaΔPDZB is sufficient to restore Gli accumulation at TCJs in salivary glands (J).

Scale bars: 20 µm (B); 10 µm (C-D); 5 µm (E-J).

Figure 7

The geometry of three-cell vertices may promote accumulation of Aka at TCJs.

(A) Schematic drawing of a three-cell vertex based on freeze-fracture electron micrographs (Graf et al., 1982). Plasma membranes of three adjoining cells are shown. Bicellular SJ septa are shown for one cell only. Near the tricellular junction (TCJ), bicellular SJ septa turn by 90 degrees to run along the apical-basal axis, forming the lateral limiting strands (LS, orange). Stacked triangular diaphragms in the TCJ central canal contact membrane corners and the three limiting strands on each side of the TCJ.

(B) Schematic view of cross-section at a three-cell vertex (adapted from Graf et al., 1982). BCJ septa are indicated in dark grey, TCJ limiting strands (LS) in orange. Gli was proposed to be associated with the limiting strands (Schulte et al., 2003). Note that dihedral angles between bicellular membranes approaching the TCJ are equal. The size and triple-repeat structure of Aka's extracellular domain suggest that the triangular diaphragms in the central canal (Graf et al., 1982) may contain Aka protein (triangular structure inside TCJ canal).

(C) The geometry of tricellular vertices could promote Aka accumulation by confining diffusion at the TCJ to one dimension (compared to two dimensions in the rest of the membrane), which can increase the probability of interaction between binding partners.

(D) Computer simulations of Aka enrichment at TCJs in the absence of external cues. The model includes synthesis, degradation, binding, dissociation, and diffusion within the plasma membrane. Aka enrichment at TCJs over time is plotted. Different colors show sensitivity to halving and doubling parameters indicated in the legend to the right. Results are mean (fat lines) +/- s.e.m. (narrow lines) from three independent simulations. Note that Aka becomes enriched 40-fold at TCJs after 2-2.5 h of simulated time, although this equilibrium is sensitive to changing parameters by two-fold.

See also Movie S1, Figure S6, and Supplemental Information for details.

Figure 1
Click here to download high resolution image

Figure 1

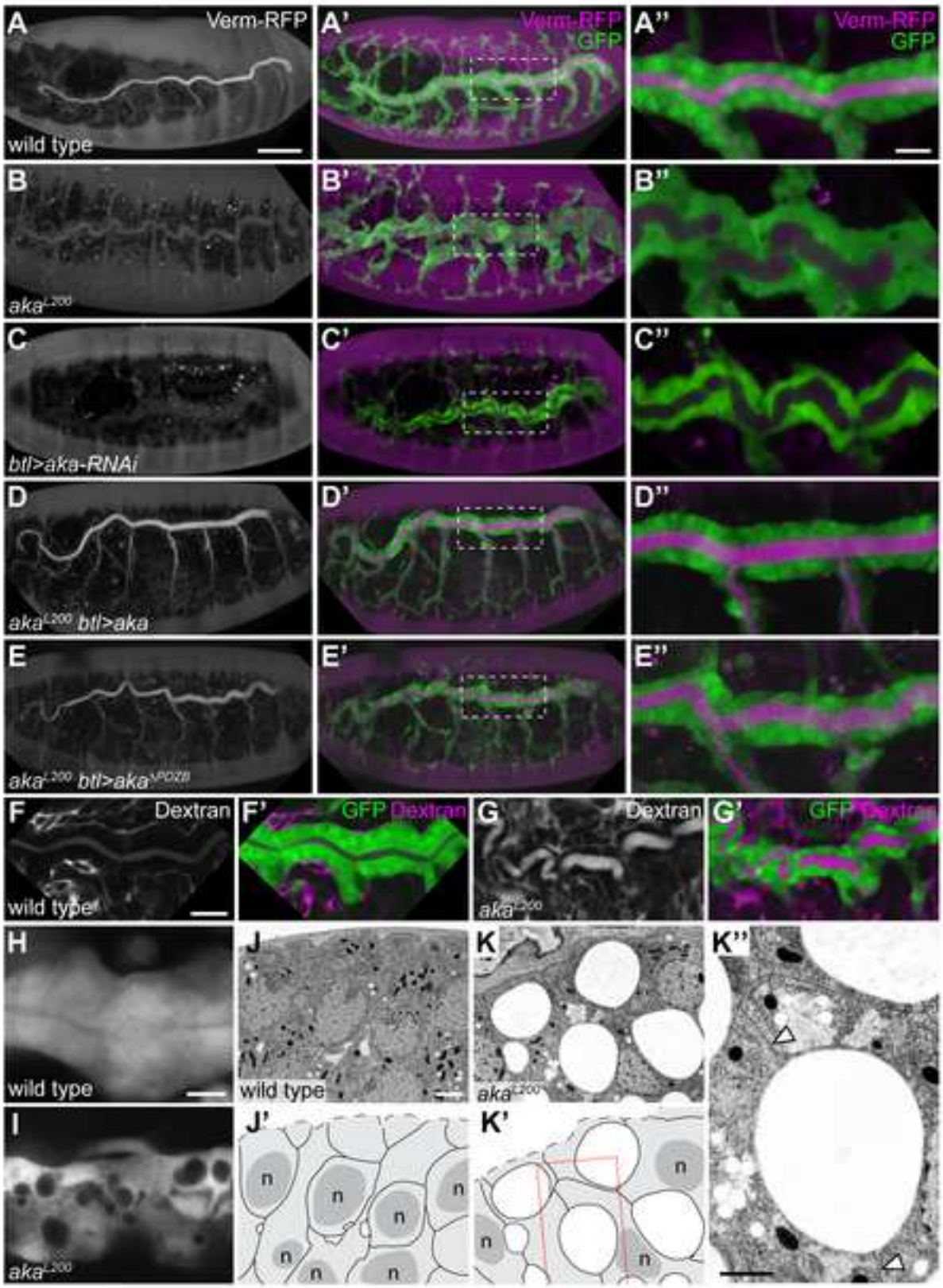

Figure 2

Click here to download high resolution image

Figure 2

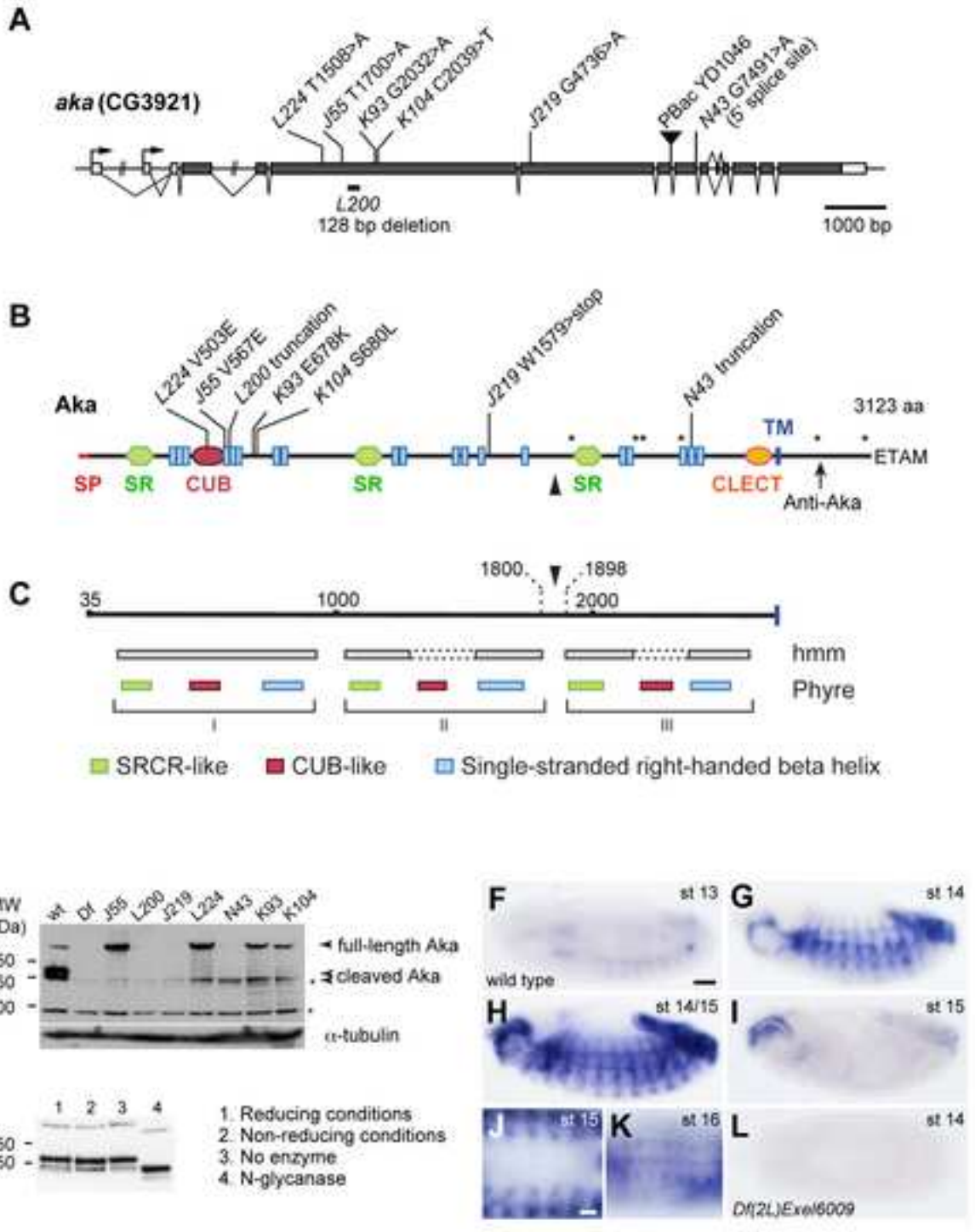

Figure 3
Click here to download high resolution image

Figure 3

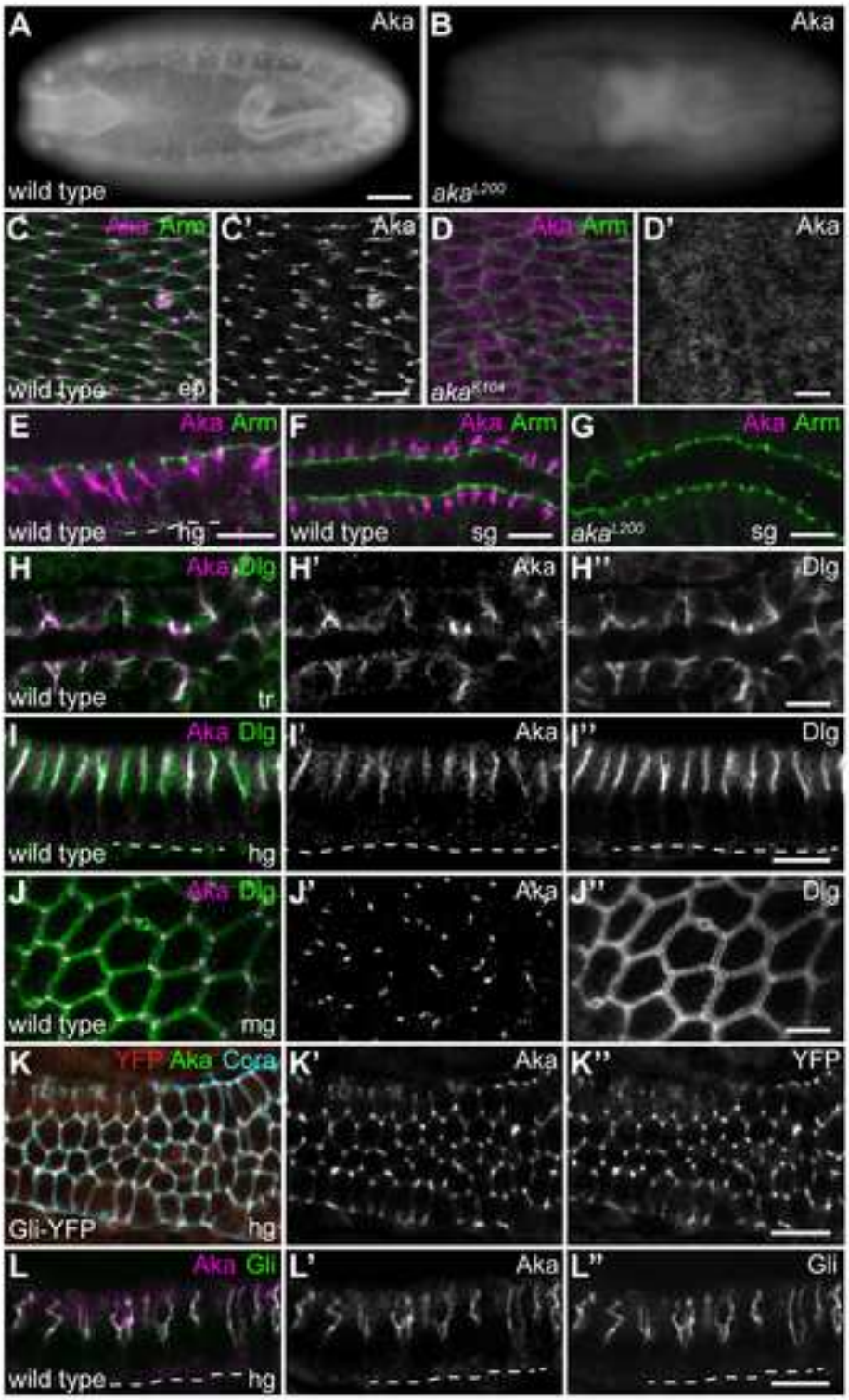

Figure 4

Click here to download high resolution image

Figure 4

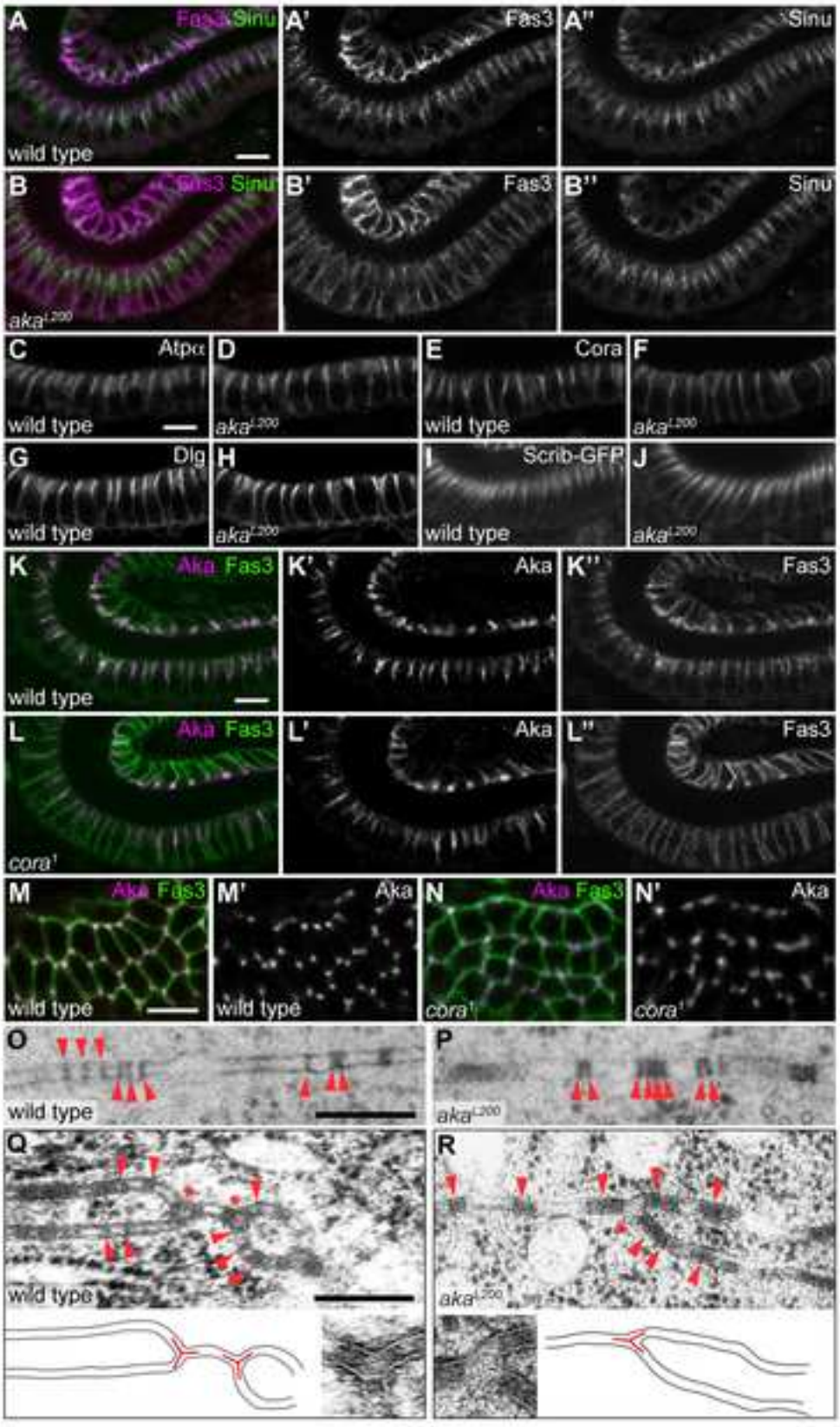

Figure 5
Click here to download high resolution image

Figure 5

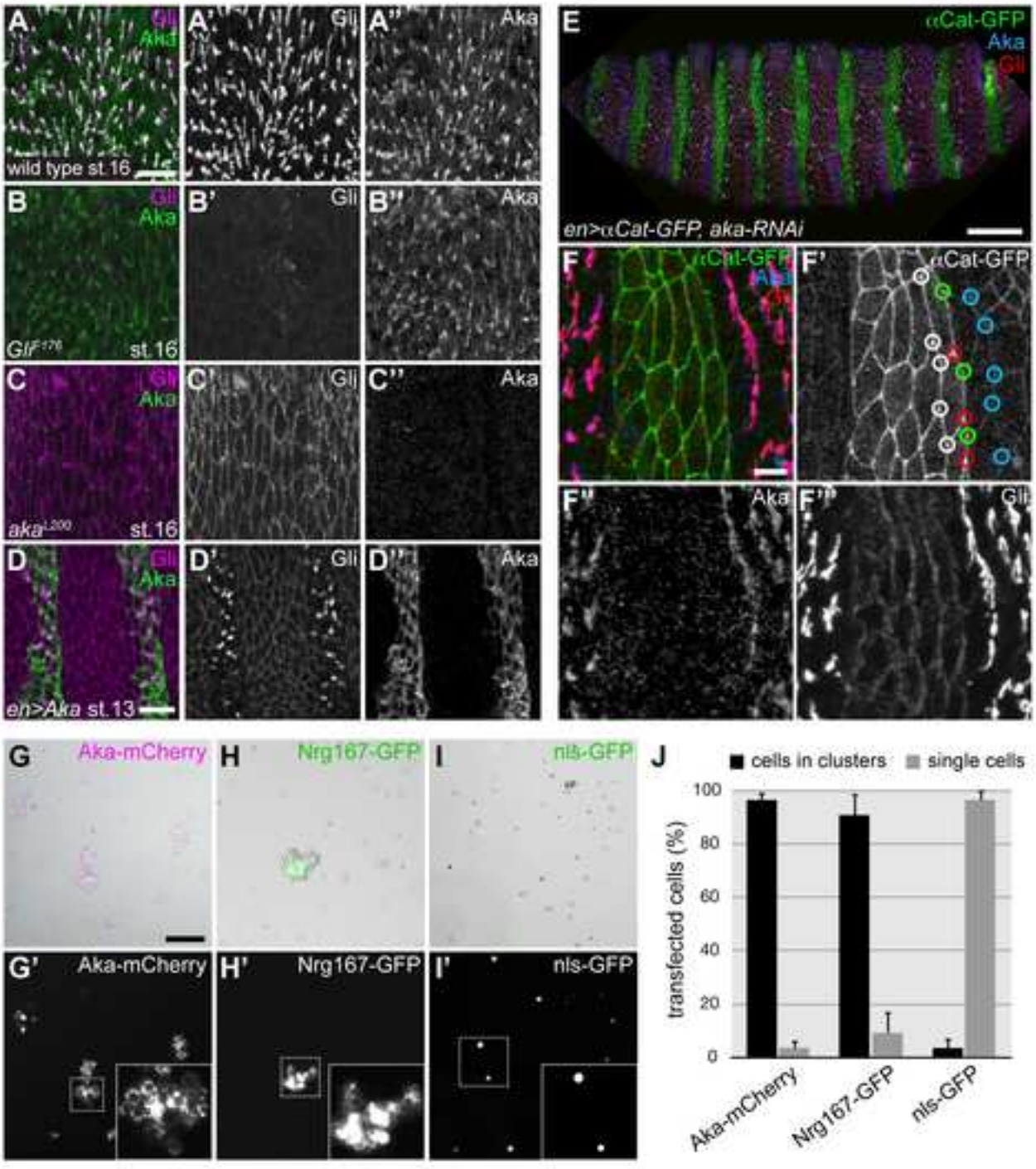

Figure 6
Click here to download high resolution image

Figure 6

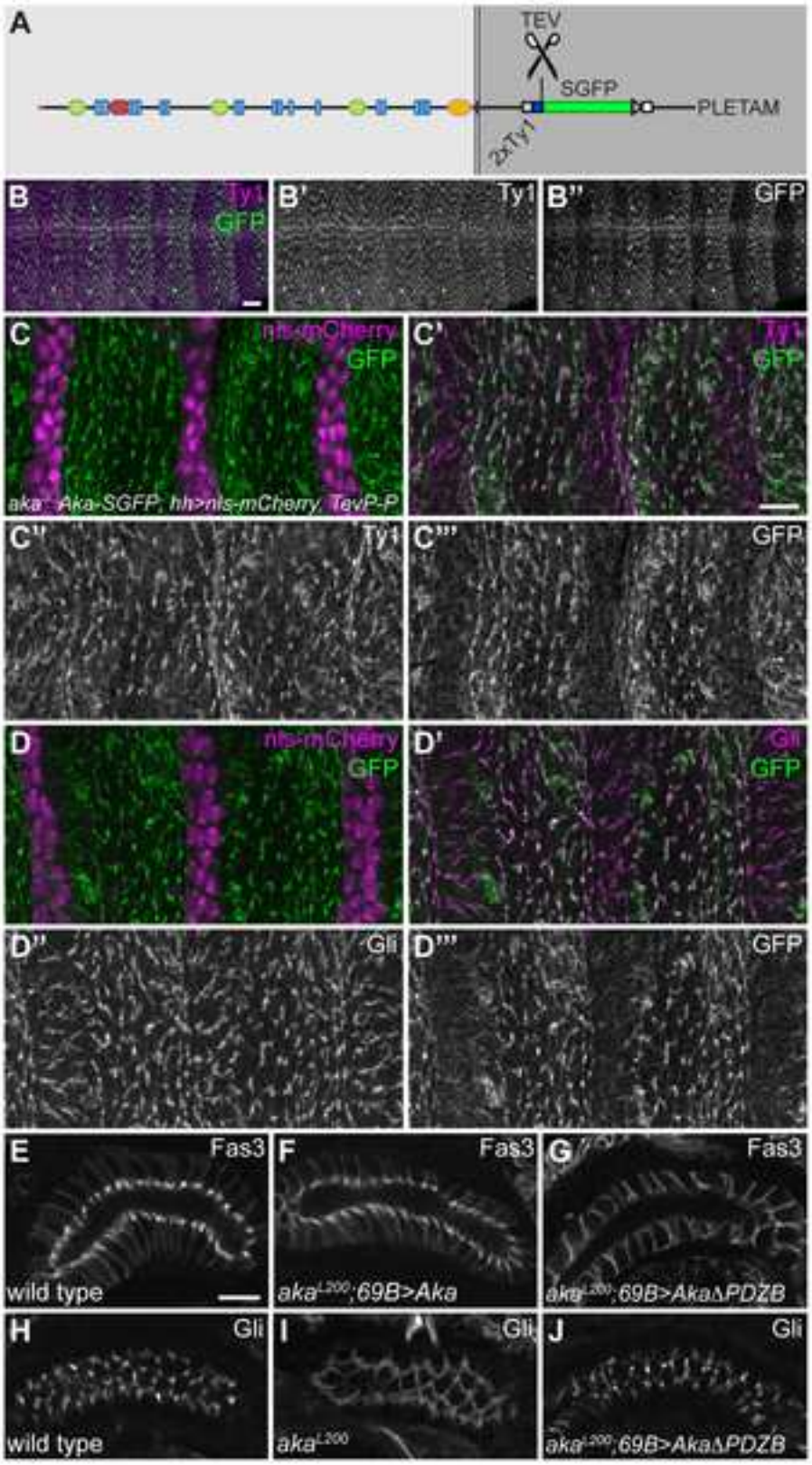

Figure 7
Click here to download high resolution image

Figure 7

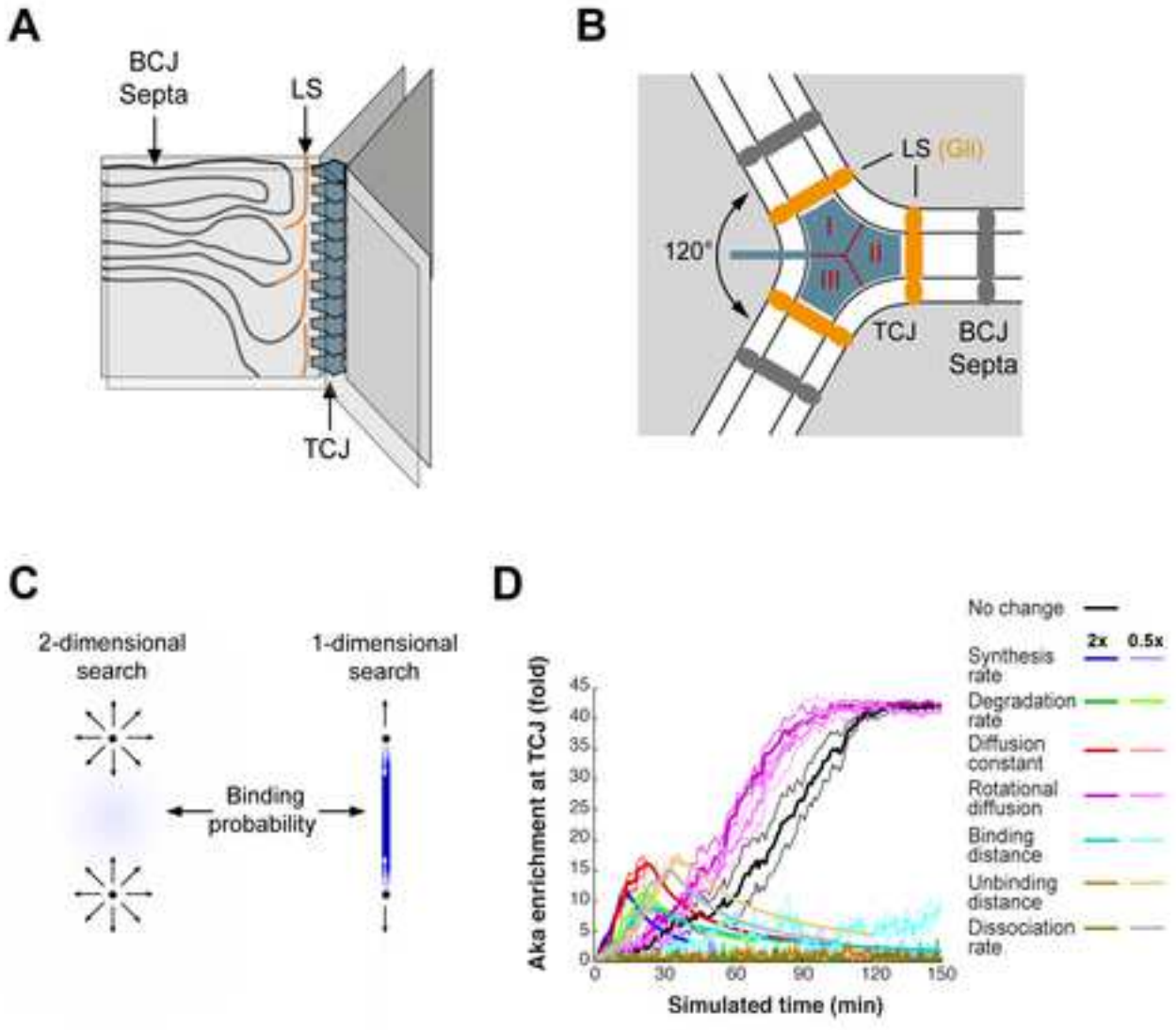

Supplemental Information

Supplemental Inventory

Supplemental Figure 1

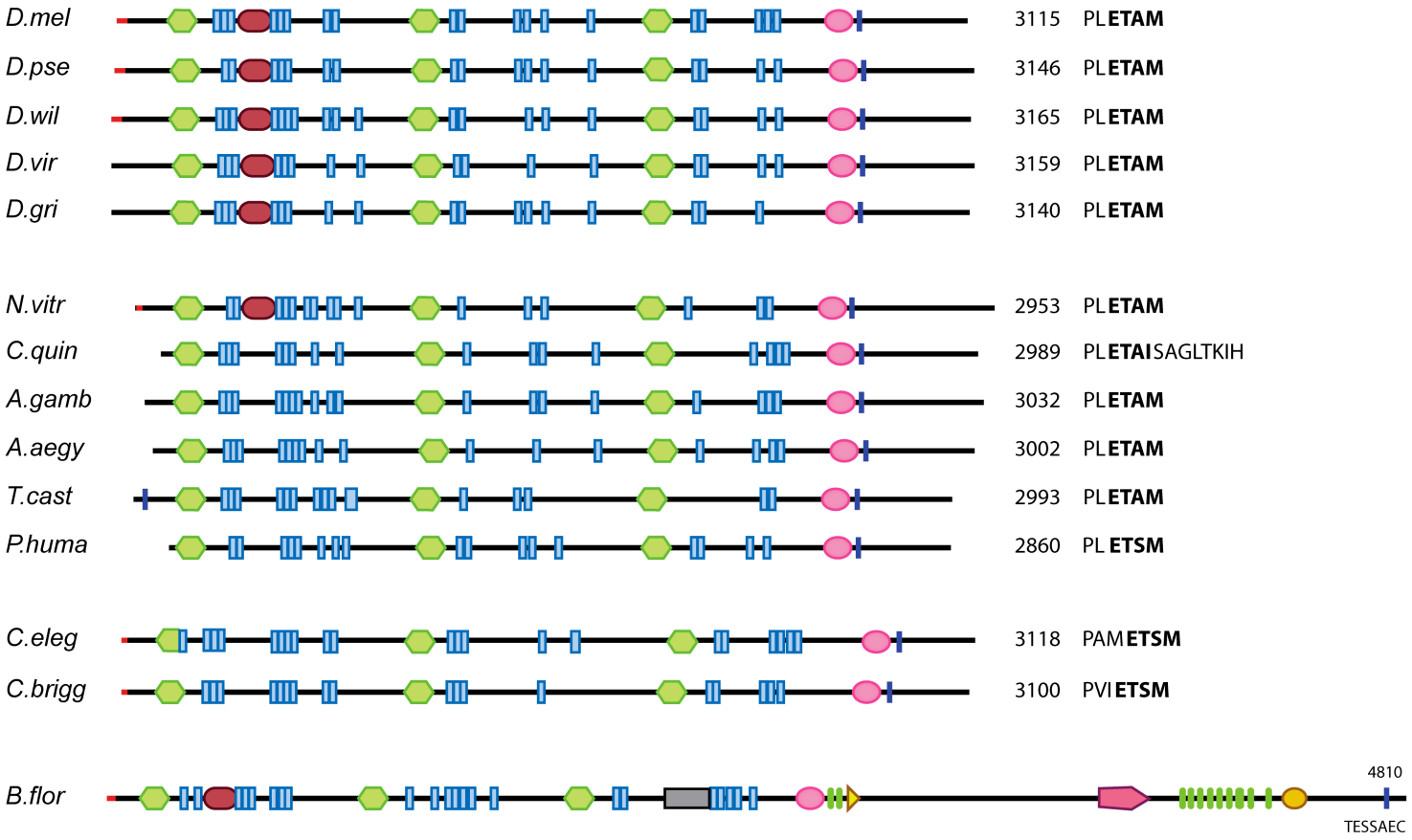

- Signal peptide
- transmembrane domain
- Scavenger receptor Cys-rich
- PbH1 (Parallel beta-helix repeat)
- CUB (*C*omplement C1r/C1s, *U*egf, *B*mp1) is a structural motif of approximately 110 aa.
- CLECT (C-type lectin or carbohydrate-recognition domain)
- MAM occurs in several cell surface proteins, including Meprins, and is thought to function as an interaction or adhesion domain.
- Epidermal growth factor-like domain (EGF)
- PSI: domain found in Plexins, Semaphorins and Integrins
- von Willebrand factor (vWF) type D domain
- Cadherin repeats

Figure S1, related to Figure 2

The tripartite repeat structure of Aka protein is evolutionarily conserved.

Predicted domain structure of Aka homologues from five Drosophilid species (*D.mel, Drosophila melanogaster; D.pse, Drosophila pseudoobscura*; *D.wil, Drosophila willistoni; D.vir, Drosophila virilis; D.Gri, Drosophila grimshawi*), six more distantly related insect species (*N.vitr, Nasonia vitripennis; C.quin, Culex quinquefasciatus*; *A.gamb, Anopheles gambiae; A.aegy, Aedes aegypti; T.cast, Tribolium castaneum; P.huma, Pediculus humanus corporis*), two nematode species (*C.eleg, Caenorhabditis elegans; C.brigg, Caenorhabditis briggsae*), and a Cephalochordate (*B.flor, Branchiostoma floridae*). Note that the number, arrangement and spacing of the repeated elements and the overall size of the extracellular domain is conserved between species. The C-terminal class I PDZ-binding motif is conserved among Aka homologues in insects and nematodes, but not in the *B. floridae* Aka homologue.

Supplemental Figure 2

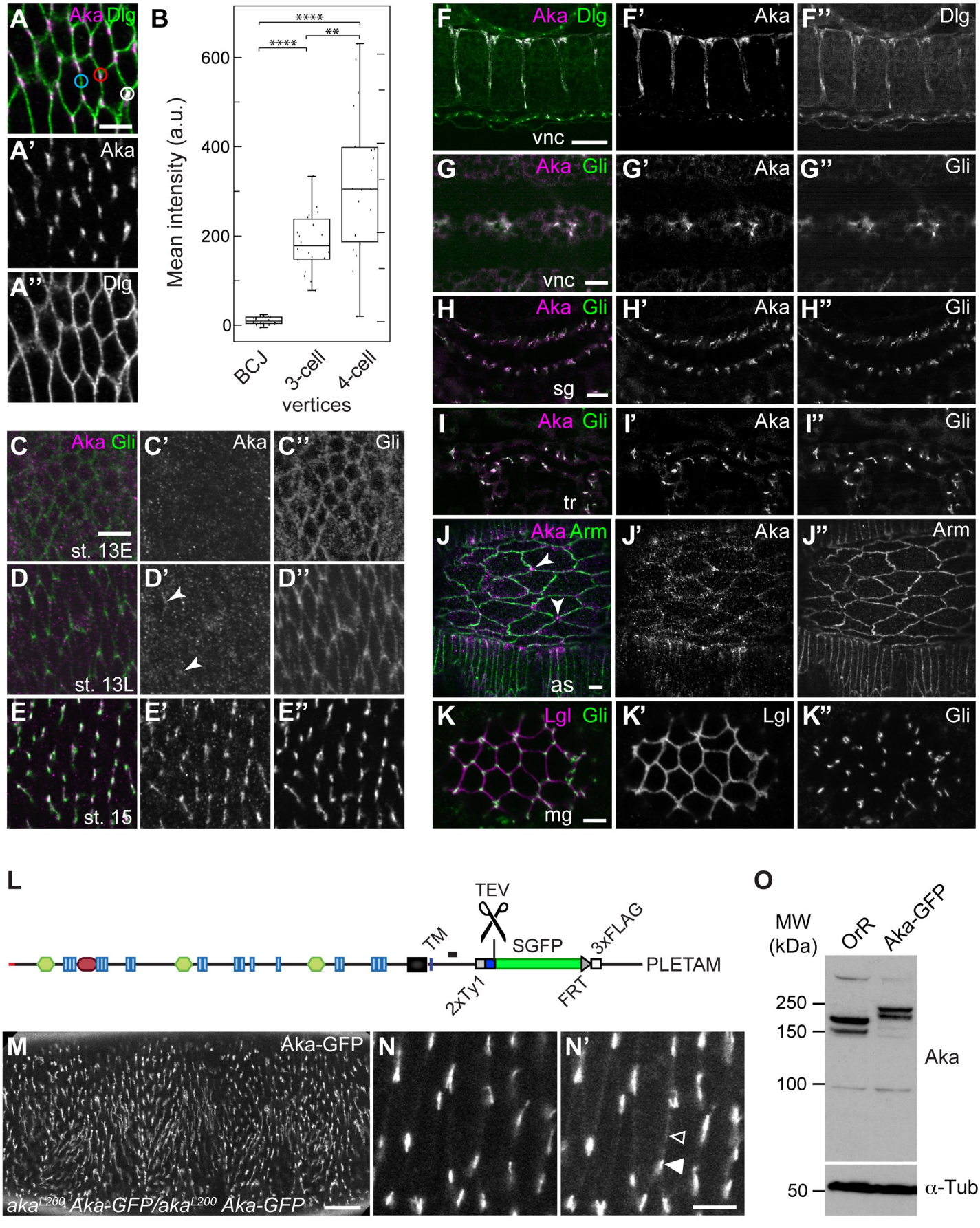

Figure S2, related to Figure 3

Localization of Aka protein and co-localization with Gliotactin.

(A-A'') Epidermis in wild-type embryo stained with anti-Aka (magenta) and anti-Dlg (green) antibodies. A bicellular junction (blue circle), a three-cell vertex (red circle) and a four-cell rosette vertex (white circle) are indicated.

(B) Quantification of Aka signals at bicellular junctions (BCJs), three-cell vertices and four-cell vertices as indicated in (A). Box plot shows minimal, maximal, and median intensities with upper and lower quartiles. Intensities were measured for least 20 junctions of each class. Mean Aka intensities at three-cell vertices were 18-fold higher compared to BCJs. Aka intensities at vertices of multicellular rosettes with more than three adjoining cells were 31-fold higher compared to BCJs. Note that multicellular vertices presumably contain multiple TCJs within a distance below the resolution limit. Asterisks indicate p-values according to Student's t-test. **: $p \leq 0.01$; ****: $p \leq 0.0001$.

(C-E'') Time course of Aka and Gli distribution from stage 13 to 15 in epidermis of wild-type embryos stained with anti-Aka (magenta) and anti-Gli (green) antibodies. Gli is distributed throughout the lateral plasma membrane at early stage 13 (C'') and begins to accumulate at cell vertices during late stage 13 (D''). Gli is strongly enriched at TCJs at stage 15 (E''). Aka is detectable as punctate intracellular staining that increases during late stage 13 (C', D'). At the same time, Gli begins to accumulate at vertices (D'). Note that elevated Gli signals at cell vertices co-localize with Aka puncta (arrowheads in D') at late stage 13. At stage 15 Aka is strongly enriched at TCJs (E'). Note that the weak punctate signals in anti-Aka immunostainings before late stage 13 cannot be distinguished from non-specific signals.

(F-F'') Lateral view of the ventral nerve cord (vnc) of a stage 17 embryo. Aka (magenta) co-localizes with Dlg (green) in clusters of cells along the midline.

(G-I'') Confocal sections of wild-type embryos co-labeled with anti-Aka (magenta) and anti-Gli (green). Ventral view of the ventral nerve cord at stage 17 shows that Aka and Gli co-localize in cells along the midline (G-G''). Cross-sections of salivary gland (sg; H-H'') and tracheal (tr; I-I'') epithelia show overlapping distribution of Aka and Gli along the apical-basal axis.

(J-J'') Dorsal view of stage 16 embryo co-labeled with anti-Aka (magenta) and anti-Arm (green) shows Aka localization at TCJs in the extra-embryonic amnioserosa (as; arrowheads).

(K-K'') *En face* view of the midgut of a stage 17 embryo labeled for Lgl (magenta) and Gli (green) shows that Gli localizes to TCJs in the endodermal midgut epithelium.

(L) Schematic representation of the Aka-Ty1-Tev-SGFP-FLAG construct. Positions of the transmembrane domain (TM), the 2xTy1 and 3xFLAG epitope tags, the Tev protease cleavage site, the SGFP coding sequence, an FRT site, and of the peptide recognized by the anti-Aka antiserum (small bar between TM and 2xTy1 tag) are indicated.

(M-N') Live imaging of *aka*^{L200} embryo (stage 16) expressing Aka-Ty1-Tev-SGFP-FLAG reveals accumulation of GFP signals at TCJs in the epidermis (M). (N) and (N') show the same close-ups of the epidermis acquired with lower (N) and higher (N') confocal gain settings. Note that at high-gain settings, Aka-GFP becomes detectable at BCJs (open arrowhead in N'), while TCJ signals (white arrowhead in N') become saturated. Flies expressing the Aka-Ty1-Tev-SGFP-FLAG construct as the only source of Aka protein are viable and fertile, indicating that the Aka-Ty1-Tev-SGFP-FLAG protein is functional.

(O) Immunoblot of protein extracts from wild-type Oregon-R (OrR) and *aka*^{L200} *Aka-Ty1-Tev-SGFP-FLAG* (Aka-GFP) embryos probed with anti-Aka (top) and anti-alpha-Tubulin (bottom) antibodies shows shift in electrophoretic mobility of Aka-GFP (right lane) compared to wild-type untagged Aka protein (left lane).

Scale bars: 5 µm (A-A'', C-E''); 15 µm (F-F''); 5 µm (G-K''); 20 µm (M); 5 µm (N, N').

Supplemental Figure 3

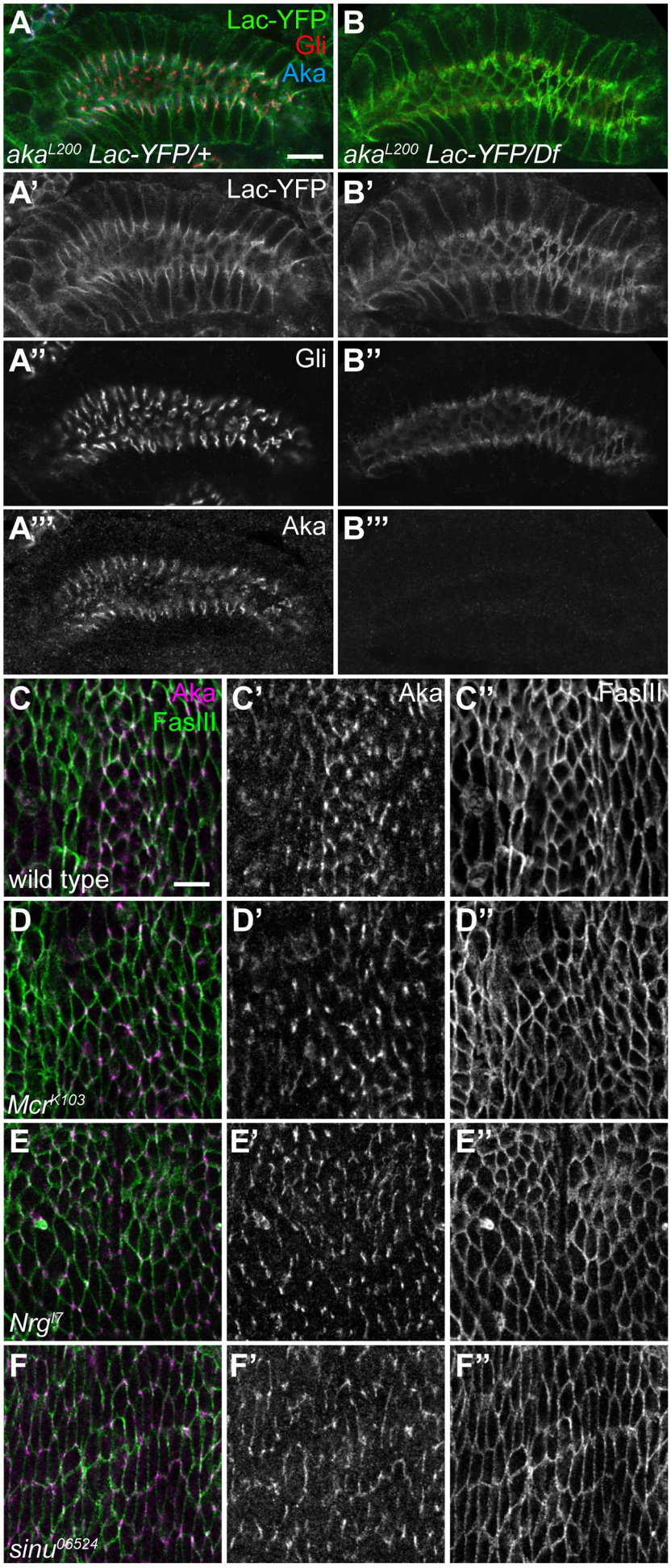

Figure S3, related to Figure 4

Localization of Aka and of bicellular septate junction proteins is mutually independent.

(A-B’’’) Confocal sections of salivary glands of control (aka^{L200}/+; A-A’’’) and aka^{L200}/*Df(2L)BSC171* (B-B’’’) embryos expressing a Lachesin-YFP (Lac-YFP) protein trap. Embryos were stained for YFP (green), Gli (red), and Aka (blue). Note that the apico-lateral accumulation of Lac-YFP in the SJ region is not affected in the absence of Aka (A’, B’), whereas accumulation of Gli at TCJs is lost and Gli instead distributes around lateral membranes (A’’, B’’).

(C-F’’’) Confocal sections of epidermis of wild-type (C-C’’), Mcr^{K103} (D-D’’), Nrg^{I7} (E-E’’), and $sinu^{06524}$ (F-F’’) embryos stained for Aka (magenta) and FasIII (green) to label cell boundaries. Note that Aka remains enriched at TCJs in Mcr^{K103}, Nrg^{I7}, and $sinu^{06524}$ mutants, in which SJs do not develop.

Scale bars: 10 µm (A-B’’’); 10 µm (C-F’’).

Supplemental Figure 4

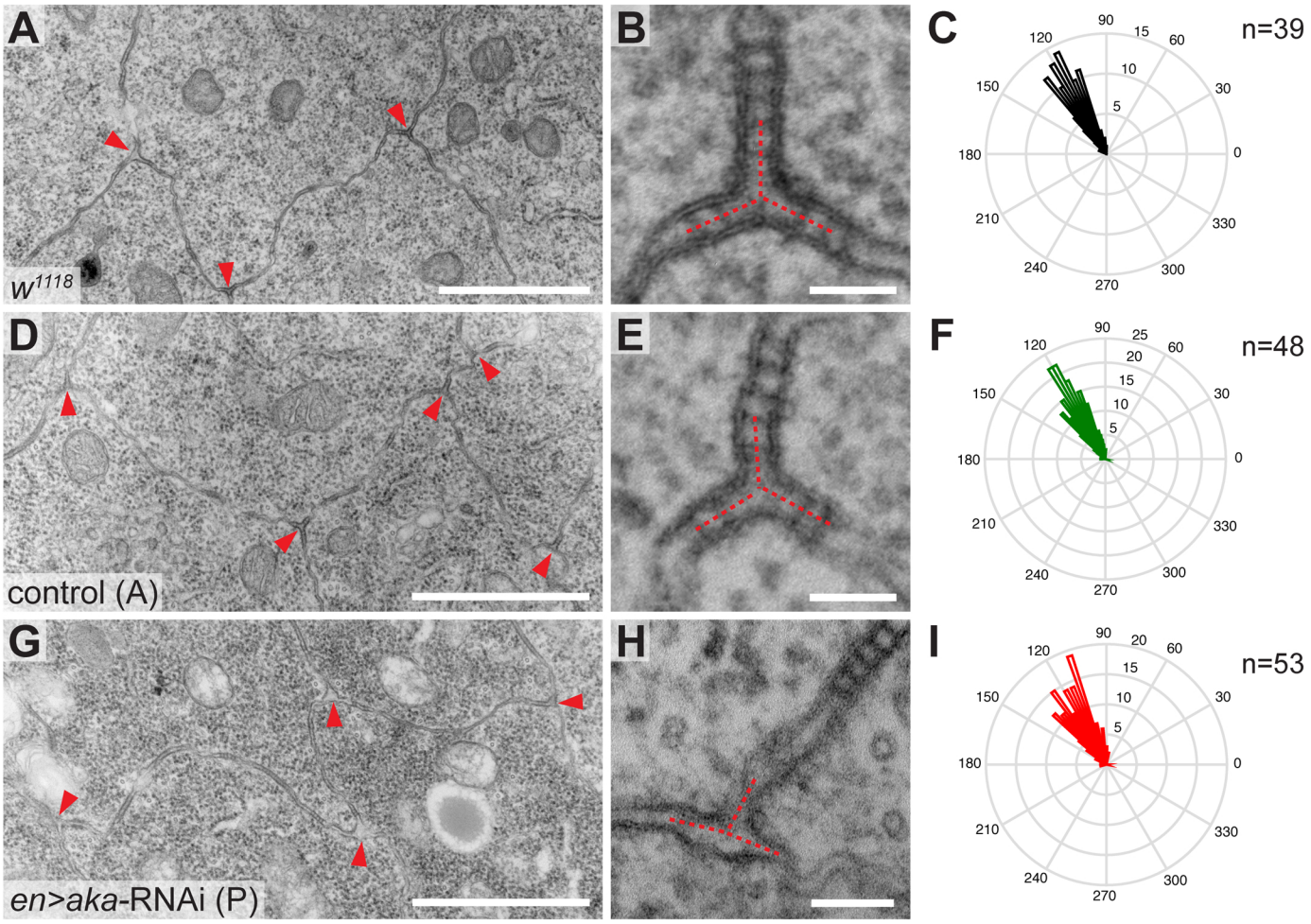

Figure S4, related to Figure 4

***aka* is required for the normal geometry of tricellular junctions.**

(A-I) Electron micrographs of third-instar wing imaginal discs sectioned in the plane of the disc epithelium. Sections shown are from a wild-type (w^{1118}) larva (A, B) and from the anterior (D, E) and posterior (G, H) compartment of a wing disc from a larva expressing aka^{RNAi} under the control of *en*-Gal4. TCJs are marked by red arrowheads in the low-magnification views (A, D, G). High-magnification views of individual TCJs are shown in (B, E, H). Note that the dihedral angles of bicellular membranes approaching a TCJ are approximately equal in the wild type (B) and in the anterior (control) compartment of the *en-Gal4 UAS-*aka^{RNAi} disc (E), but are frequently irregular in the posterior compartment of the *en-Gal4 UAS-*aka^{RNAi} disc (H). Broken red lines highlight dihedral angles of bicellular membranes at TCJs. Angle histograms (C, F, I) show the distribution of angles measured for each group. n indicates the number of TCJs analyzed per genotype (with three angles measured for each TCJ). Note that *aka*-depleted cells (G-I) show irregular TCJs and a broader distribution of dihedral angles compared to the internal control (D-F) and to the wild type (A-C).

(J) Schematic wing imaginal disc with the anterior (A, green) and posterior (P, orange) compartment highlighted. Boxes show the approximate location of regions analyzed by electron microscopy.

(K) Low-magnification overview of sectioned wing imaginal disc. Boxes indicate the approximate location of regions analyzed at higher magnification.

(L) Box plot showing Shannon entropies of TCJ angles for the control group (anterior compartment, green) and the *aka* RNAi group (posterior compartment, orange). Entropy describes the uniformity of the angle distribution, with higher entropy values corresponding to a more uniform (120°/120°/120°) angle distribution. Entropy in the *aka* RNAi group is significantly lower compared to the control group, as determined by a Mann-Whitney test (P=0.00482).

Scale bars: 1 µm (A, D, G); 50 nm (B, E, H); 100 µm (K).

Supplemental Figure 5

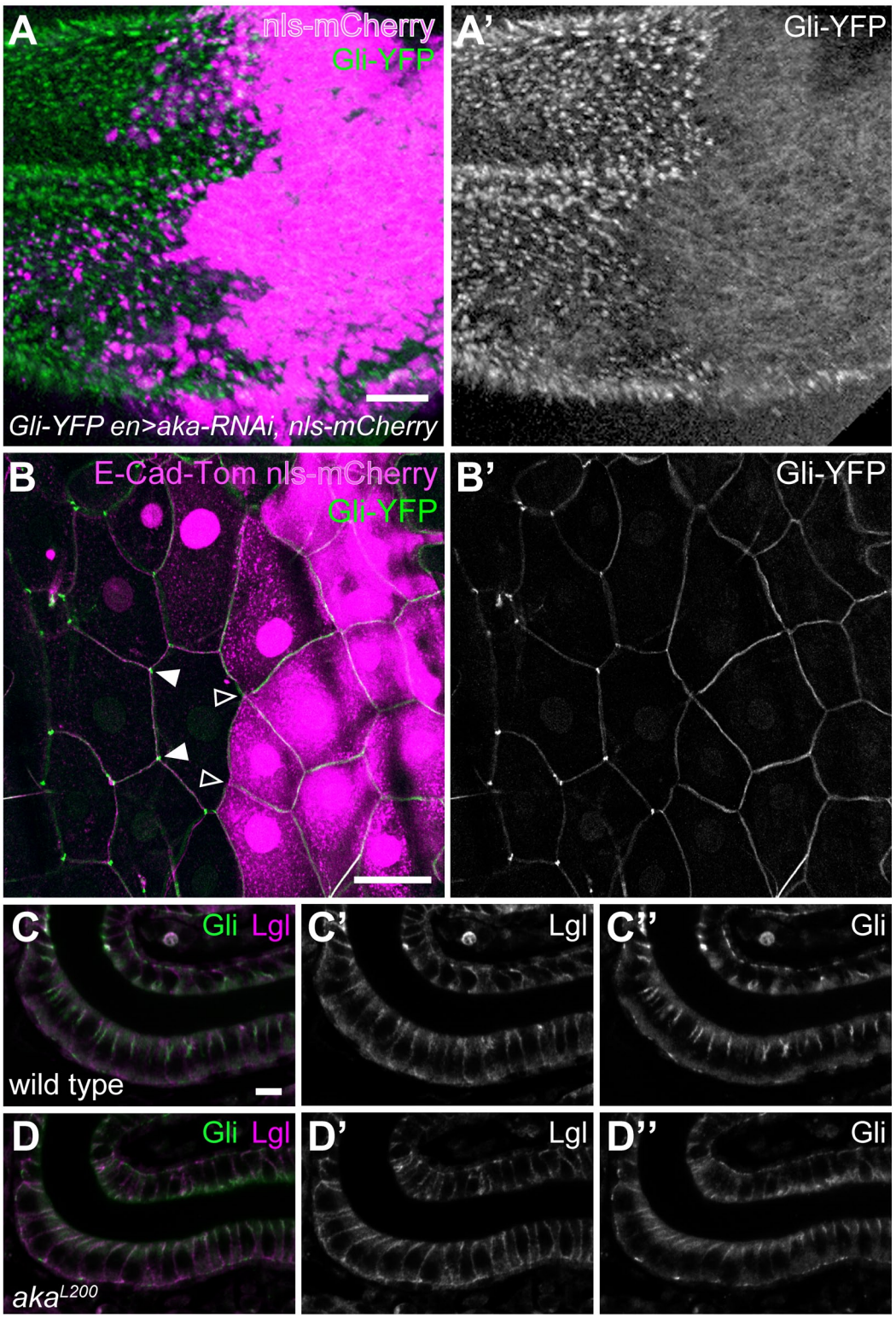

Figure S5, related to Figure 5

Aka is required for tricellular accumulation, but not apico-lateral localization of Gliotactin.

(A) Wing imaginal disc from a third-instar larva expressing Gli-YFP (green) throughout the disc. aka^{RNAi} was expressed in the posterior compartment under the control of *en*-Gal4. The aka^{RNAi} expressing cells are labeled by co-expression of nls-mCherry (magenta). Note that Gli-YFP accumulates at cell vertices in the anterior compartment, whereas Gli-YFP is mislocalized in the aka^{RNAi} expressing posterior compartment. Nuclei with faint nls-mCherry signals (left to the middle) are from the peripodial membrane overlying the disc proper cells. Anterior is to the left.

(B) Epidermis of third-instar larva expressing nls-mCherry (magenta) and aka^{RNAi} in stripes of cells under the control of *en-Gal4*. E-Cad-mTomato (E-Cad-Tom; magenta) and Gli-YFP (green) are expressed throughout the epidermis. Gli-YFP accumulates at TCJs in unperturbed control cells, whereas Gli-YFP distributes along BCJs in aka^{RNAi} expressing cells. Note that Gli-YFP accumulates at TCJs when Aka expression in all three cells abutting a TCJ is unperturbed (white arrowheads), whereas Gli-YFP accumulation at TCJs is reduced or lost when Aka is depleted from one or more cells adjoining a three-cell vertex (open arrowheads).

(C-D'') Confocal section of the hindgut epithelium of stage 16 embryos labeled with Anti-Gli (green) and anti-Lgl (magenta). Gli and Lgl retain their apico-lateral localization in aka^{L200} mutant embryos (D), as compared to the wild-type control (C).

Scale bars: 50 µm (A-B'); 5 µm (C-D'').

Supplemental Figure 6

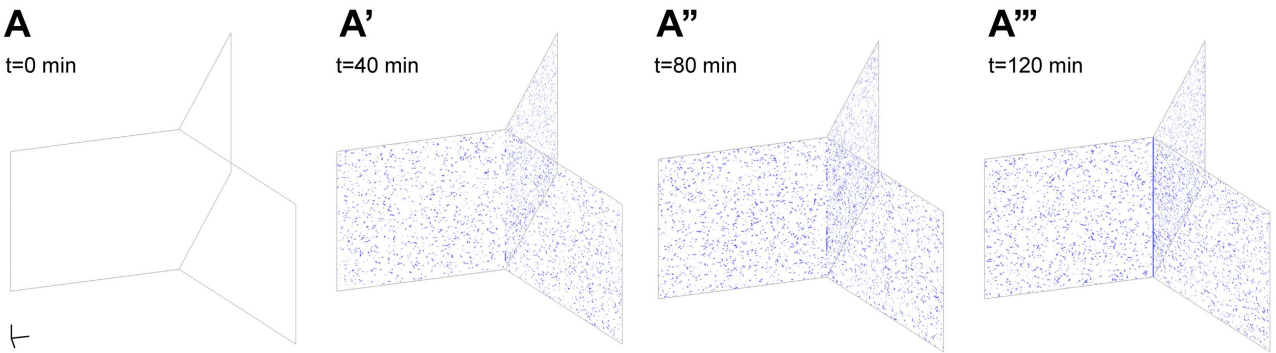

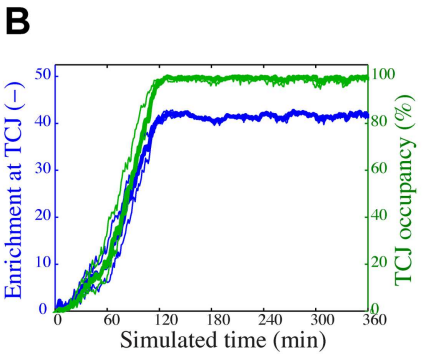

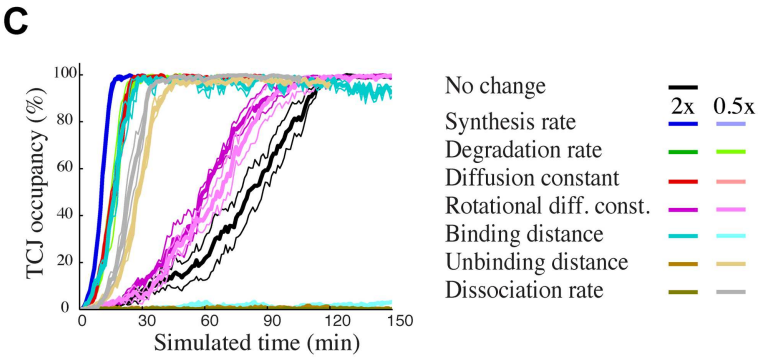

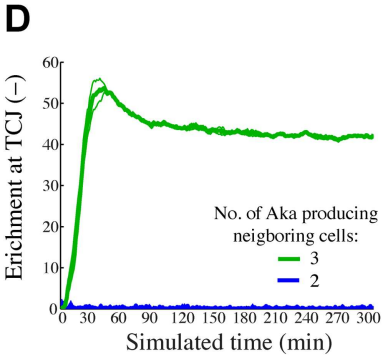

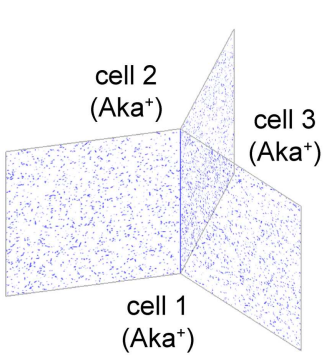

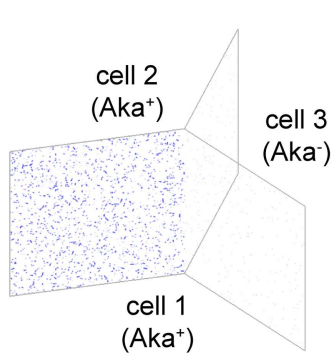

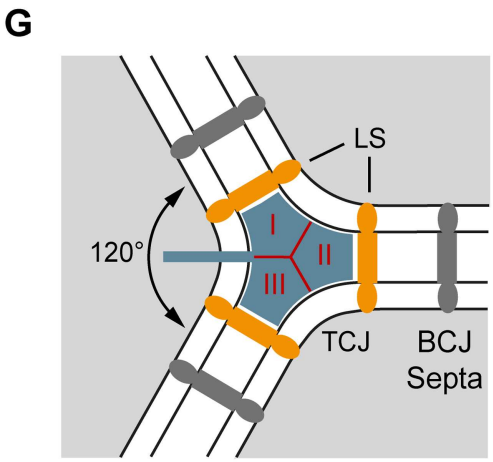

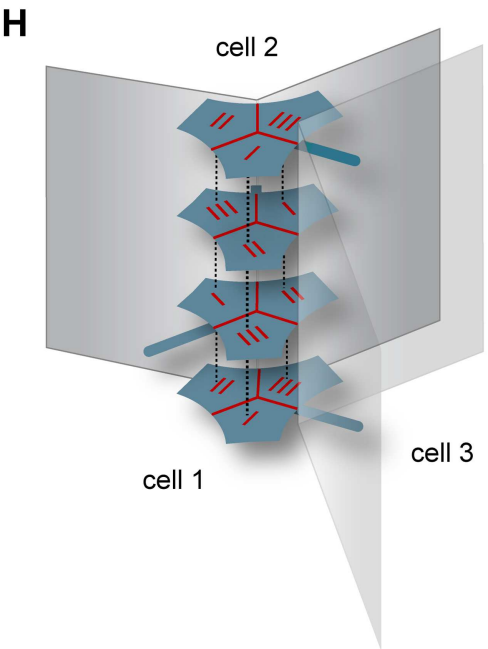

Figure S6, related to Figure 7

Simulation of Aka protein accumulation at tricellular junctions in the absence of external cues and hypothetical model of Aka protein arrangement at tricellular junctions.

(A-A''') Simulation results of four consecutive time points of the basic model that leads to accumulation of Aka at the TCJ. The scale bar (lower left) denotes 1 µm in each dimension.

(B) Running the model for extended time (360 min) indicates that equilibrium is being established.

(C) Effects on TCJ occupancy upon halving and doubling parameters of the model.

(D) Comparison of Aka enrichment at the TCJ between a model that includes three Aka producing adjoining cells (green curve) and a model with two Aka-producing cells (blue curve). The model was the same as the basic model, except for the dissociation constant at the TCJ, which was set to zero. Note that even in this extreme case of Aka complex stability at the TCJ, there is hardly any TCJ enrichment of Aka when only two neighboring cells produce Aka.

(E-F) Visualizations of single simulations from (D) after five hours. (E) shows a situation in which Aka is produced by all three adjoining cells, while in (F) Aka is produced by two cells (cell 1 and 2) only. Note that in the model a higher concentration of Aka leads to more binding, which then decreases degradation. This explains why in (F) Aka signals at the bicellular membranes of Aka-producing cells 1 and 2 are more than two-fold higher compared to the bicellular membranes shared with the non-producing cell (3).

Results in (B-D) are means +/- s.e.m. from three independent simulations. Values are plotted every simulated minute. Abbreviations: t: simulated time; diff. const.: diffusion constant.

(G) Cross-sectional view of a three-cell vertex (adapted from Graf et al., 1982). BCJ septa are indicated in dark grey, TCJ limiting strands (LS) are indicated in orange.

(H) Hypothetical model of Aka arrangement at TCJs. The inferred size of full-length Aka protein and the triple-repeat structure of Aka's extracellular domain suggest that a single Aka protein may span the TCJ canal (25-30 nm; Graf et al., 1982; Noirot-Timothee et al., 1982) and interact with binding partners on three membranes. In addition, the finding that TCJ formation requires Aka expression in all three cells adjoining a tricellular vertex suggests that Aka molecules from three adjoining cells interact either directly or indirectly with each other. Note that regular stacking of Aka molecules produced by three adjoining cells would imply the formation of a helicoidal stack of proteins, with an offset of either 120 or 240 degrees between adjacent molecules in the stack. Aka repeat regions are indicated (I-III). For clarity, plasma membranes are shown for two cells only.

Movie S1, related to Figure 7

Simulation results of a model that does not contain any external cues for directing Aka to the TCJ. An image was generated every 20 simulated seconds. The scale of axes is in μm. See Supplemental Experimental Procedures for details.

Supplemental Experimental Procedures

Isolation of *aka* mutants

The mutagenesis screen will be described in detail elsewhere. In brief, males carrying a second chromosome marked with *btl-Gal4, UAS-GFP* and *UAS-Verm-RFP* transgenes were mutagenized by EMS (25 mM) feeding as described in (Luschnig *et al*., 2004). 4,800 lines were established from single F1 males by balancing the mutagenized chromosomes over the *CyO Dfd-GMR-nvYFP* chromosome (Le *et al.*, 2006). Living F3 embryos were scored for tracheal morphology and for Verm-RFP accumulation in the tracheal lumen. Homozygous embryos were identified by the absence of the Dfd-GMR-nvYFP marker. 139 lines that showed penetrant tracheal defects were kept and were classified according to their phenotypes. Mutants showing similar phenotypes were crossed to test for complementation of lethality. One complementation group with nine lethal alleles was named *anakonda* (*aka*) based on the tortuous tracheal tube phenotype of the mutant embryos. The embryonic defects of all nine EMS-induced *aka* alleles were similar in strength. Hemizygous aka^{L200}*/Df(2L)Exel6009* embryos and aka^{L200} homozygotes showed defects of similar strength, indicating that aka^{L200} is an amorphic (strong loss-of-function) mutation. The aka^{L200} mutant was crossed to a panel of 110 chromosomal deficiencies that together uncover 95% of the second chromosome (FlyBase). The *aka* locus was mapped to the cytological interval 24C3-24C6 by non-complementation of *Df(2L)ED1*, *Df(2L)BSC171* and *Df(2L)Exel6009*, and by complementation of *Df(2L)ED247*. Testing mutations in candidate genes in this region revealed that the *PBac*(*YD1046*) insertion (Quinones-Coello *et al.*, 2007) in the CG3921 gene failed to complement all nine *aka* alleles. The aka^{L200} mutation was recombined onto an FRT40A chromosome to remove associated mutations, as well as the *btl-Gal4, UAS-GFP* and *UAS-Verm-RFP* transgenes.

Molecular Biology and constructs

Genomic DNA was extracted from 20 homozygous *aka* embryos identified by the absence of *CyO Dfd-YFP*. The *aka* coding sequence, including exon-intron boundaries, was amplified from *aka* mutants and from the parental strain. PCR products were sequenced on both strands.

The UAS-Aka construct was generated by amplifying the genomic *aka* coding region from fosmid clone FlyFos028221 (Ejsmont *et al.*, 2009) using oligonucleotides Aka-F-NotI (5'-GCGGCCGCGAAACTGCCATGGCGAATGTG) and Aka-R-NheI (5'-GCTAGCCTACGAAGCTGTGGTGGTTGT). The PCR product was cut with NotI and NheI and inserted into pUASTattB using NotI and XbaI. UAS-Aka-deltaPDZB was generated analogously, except that the reverse primer (5'-GCTAGCTCACAGGGGCTGACTGTGACTTCG) was designed to omit the last four codons corresponding to the PDZ-binding motif (ETAM). UAS-Aka-mCherry was

generated by inserting a synthesized cassette (ShineGene, Shanghai, China) consisting of a 2xHA tag, a TEV protease cleavage site and the mCherry ORF into the *aka* coding region 72 bases upstream of the stop codon. Inserts were confirmed by sequencing before PhiC31 integrase-mediated integration into the P[CaryP]attP2 landing site at 68A4 (BestGene, CA, USA).

Fosmid recombineering

Fosmid recombineering was performed as described (Ejsmont *et al.*, 2009). FlyFos clone 028221, which contains 9540 bp upstream and 12530 bp downstream of the *aka* gene, was modified by inserting a cassette containing a 2xTy1 epitope tag, a Tev protease cleavage site, the superfolder-GFP (SGFP; Pedelacq *et al.*, 2006) coding sequence, and a 3xFLAG epitope tag (2xTy1-Tev-SGFP-3xFLAG; gift from P. Tomancak, Dresden, Germany; Ejsmont *et al.*, 2009) 72 bases upstream of the *aka* stop codon. The *aka* coding sequence in the tagged fosmid was confirmed by sequencing. The fosmid was integrated into P[CaryP]attP40 (25C6) and recombined with *Df(2L)Excel6009*. Flies carrying the *Aka-Ty1-Tev-SGFP-FLAG Df(2L)Excel6009* chromosome in trans to *aka* mutations were viable and fertile, indicating that the Aka-Ty1-Tev-SGFP-FLAG fusion protein is functional.

Light microscopy and image analysis

Imaging was performed using an Olympus FV1000 confocal microscope with 40x/1.3 NA and 60x/1.35 NA objectives. Images were processed using Huygens Deconvolution (SVI), ImageJ (v1.42), Imaris (v7.3.0; Bitplane) and Adobe Photoshop. For live imaging, dechorionated embryos were mounted on glue-coated coverslips and covered with Voltalef 10S oil. Aka signals were quantified on single confocal sections using circular regions of interest (ROIs) in ImageJ. ROIs were placed on bicellular junctions, three-cell vertices, or four-cell vertices using anti-Dlg staining as a marker for cell boundaries. Aka signals were measured in these ROIs. Background (measured in a ROI in the cell center) was subtracted from mean Aka intensities for each cell boundary ROI. At least 20 junctions of each type (bicellular junctions, tricellular vertices, multicellular rosette vertices) were analyzed.

Electron microscopy

Staged living embryos within the vitelline membrane were frozen in 1-hexadecene with a high-pressure freezer (Bal-Tec HPM 010; Balzers, Liechtenstein). After fixation through freeze-substitution (glutaraldehyde, osmium tetroxide and uranyl acetate), embryos were embedded in Epon, sectioned (50 to 70 nm), contrasted (lead citrate and uranyl acetate) and imaged in a Philips CM10 electron microscope. Wing imaginal discs were dissected from third instar larvae, immediately fixed in 0.1M phosphate buffer (pH 7.0) containing 4% paraformaldehyde and 0.5% glutaraldehyde at room

temperature for at least 2 h and subsequently stored at 4°C over night. After fixation (2% osmium tetroxide for 1 h on ice, 2% uranyl acetate for 30 minutes at room temperature), discs were dehydrated, embedded in Epon, sectioned (70-85 nm), contrasted (2% uranyl acetate for 30 minutes, 0.4% lead citrate for 3 minutes) and imaged in a Zeiss EM 900 with an Olympus SIS Morada digital camera.

Analysis of dihedral angles at tricellular junctions

For analysis of TCJ angles, wing imaginal discs from *UAS-dicer2/+; en-Gal4 UAS-mCherry-nls/+; UAS-aka-RNAi/+* larvae were observed prior to osmium fixation in a fluorescent stereomicroscope to check the expression of mCherry-nls in the posterior compartment. For electron microscopy, low-magnification overviews were used for orientation. Close-ups were taken from regions of the posterior (expressing *aka* RNAi) and anterior (internal control) wing pouch. Five wing discs from three animals were analyzed. For statistical analyses, all three angles between bicellular membranes approaching a TCJ were determined using the iTEM Software (Olympus SIS). Angle distributions were plotted as angle histograms in MatLab. In addition, we calculated for each set of angles the Shannon entropy (http://en.wikipedia.org/wiki/Entropy_in_thermodynamics_and_information_theory). Entropy describes the uniformity of the angle distribution, with higher entropy values corresponding to a more uniform (120°/120°/120°) angle distribution. We compared the control group and the *aka* RNAi group using a Mann-Whitney test.

***In situ* hybridization**

Whole-mount *in situ* hybridization was performed with digoxigenin-labeled RNA antisense probes as previously described (Tonning *et al.*, 2005). RNA probes were generated from PCR products, where the reverse primer contains a T7 polymerase promoter sequence (TAATACGACTCACTATAGG). Probes made from two different PCR templates (*aka* exons 4 and 5) gave indistinguishable results. Antibody detection of GFP produced from the balancer chromosome to identify *Df(2L)Exel6009* homozygous embryos deficient for aka was performed prior to in situ hybridization.

Protein sequence analyses

Multiple aligments by ClustalW2 (http://www.ebi.ac.uk/Tools/msa/clustalw2/) included the predicted Aka homologues from *D. melanogaster* (CG3921-PA), *A. gambiae* (AGAP009143-PA), *T. castaneum* (TC007861), *N. vitripennis* (NV11387-PA), *A. pisum* (np5qh9), *D. pulex* (3ffjxn), *C. elegans* (GN=C06B8.7) and *B. floridae* (C3XRZ4). The output alignments were converted to Stockholm format (http://sequenceconversion.bugaco.com/converter/biology/sequences/) and submitted for hmmsearch (http://hmmer.janelia.org/search/hmmsearch). Phyre V2.0 was used for protein structure predictions (Kelley and Sternberg, 2009).

Immunoprecipitations

Immunoprecipitations were performed with Dynabeads® co-immunoprecipitation kit (Life Technologies) according to the manufacturer's instructions. In brief, wild-type embryos (1-1.5 g; stage 15-16) were dechorionated with 2.5% sodium hypochlorite for 5 minutes at room temperature. All subsequent steps were carried out at 4°C. Dechorionated embryos were homogenized in 2.5 ml of lysis buffer (supplemented with 150 mM NaCl, 2 mM $MgCl_2$, 1 mM DTT, 1% NP-40, 2x Halt Protease and Phosphatase Inhibitor cocktail EDTA-Free (Thermo Scientific Pierce)) in a Dounce homogenizer. The lysate was centrifuged at 2600 x g for 5 minutes to pellet cell debris. The supernatant was incubated with anti-Aka-coupled Dynabeads for 30 minutes. Subsequent washes and elution was performed according to the manufacturer's protocol.

Protein in-gel digestion and MS/MS analysis

To determine the identity of shorter Aka protein isoforms, we analyzed the immunoprecipitated Aka protein by tandem mass spectrometry (MS/MS). In the first analysis, the proteins from IP eluate were in-gel digested with trypsin. The gel bands were destained by washing three times in 25 mM NH_4HCO_3 in 50% CH_3CN and one time in 25 mM NH_4HCO_3 in 50% CH_3OH. Gel pieces were dried in a vacuum centrifuge and incubated with digestion buffer (50mM NH_4HCO_3, 10 ng/µl trypsin) at 37°C overnight. Peptides were extracted in 50% CH_3CN / 1% CH_3COOH and the supernatant was evaporated to dryness in a vacuum centrifuge. Prior to MS analysis, the peptides were reconstituted in 0.2% HCOOH / 3% CH_3CN.

The peptides were analyzed on an Orbitrap Fusion Tribrid instrument (Thermo Scientific) interfaced with an in-house constructed nano-LC column. Sample injections were made with an Easy-nLC 1000 autosampler (Thermo Scientific), running at 200 nl/min. The peptides were trapped on a precolumn (45 x 0.075 mm i.d.) and separated on a reversed phase column, 25 x 0.075 mm, packed in-house with 1.9 µm Reprosil-Pur C18-AQ particles. The gradient was 7-80% CH_3CN in 0.2% HCOOH and spray voltage 1.6 kV. The Orbitrap Fusion Tribrid was operated in a data-dependent mode with the most abundant doubly or multiply charged precursors in each MS scan, 120K m/z 400-1500, selected for fragmentation (MS/MS) with CID (collision induced dissociation) at 30% and detection in the ion trap. MS/MS data were matched against the CG3921 amino acid sequence, using Proteome Discoverer 1.4, allowing semi-tryptic cleavages, with MS tolerance of 10 ppm and 0.5 Da for fragment ions.

Protein labeling, filter digestion and MS/MS analysis

In the second analysis, the proteins from IP eluate were labeled with an amine reactive tag (TMT-131, Thermo Scientific Pierce), binding to lysine and free N-terminals, including biologically cleaved

proteins. Labeling was performed in 2% SDS, 50mM TEAB (triethyl ammonium bicarbonate) and at least 40% CH_3CN according to the manufacturer. Proteins were then washed and digested with trypsin using the filter-aided sample preparation (FASP) method on Nanosep 30k Omega filters (Pall Life Sciences, modified from Wisniewski *et al.*, 2009). Peptides were extracted, desalted using C18 spin columns (Thermo Scientific Pierce), eluted, dried and reconstituted in 0.2% HCOOH / 3% CH_3CN.

The peptides were analyzed on a QExactive instrument (Thermo Scientific) interfaced with an in-house constructed nano-LC column as described above. The QExactive was operated in a data-dependent mode with the ten most abundant doubly or multiply charged precursors in each MS scan, 70K m/z 400-1600, selected for fragmentation (MS/MS) with HCD (higher energy collision dissociation) at 30%. MS/MS data were matched against the CG3921 amino acid sequence, using Proteome Discoverer 1.4, allowing semi-tryptic cleavages, dynamic modification of TMT reagent, MS tolerance of 5 ppm and 0.1 Da for fragment ions.

Computer simulations

Aka localization was modeled stochastically, where each molecule was represented explicitly. The time step was kept constant. Initially, no molecules are present. The processes being modeled are synthesis, degradation, diffusion, binding to form homomultimeric complexes, and dissociation of these complexes. The geometry on which the processes are modeled is shown in Figure S6. Three parts of membranes are modeled, each belonging to a different cell, thereby including the TCJ and half of the adjacent bicellular junction forming membranes. Each molecule belongs to one of the three cells and it can only diffuse within the membrane of this cell. This means that after binding of two molecules from two different cells, diffusion is limited to the region where the membranes of these two cells contact. In addition, a multimeric complex, which contains molecules of three different cells, is restricted to the TCJ.

Synthesis

Synthesis in the model means the disposition of molecules to one of the membranes. In the cell, this can correspond to protein synthesis, but may also be part of a dynamic system, where molecules are, for example, recycled through endo- and exocytosis.

Synthesis is assumed to be a zero-order reaction, where the time dependence of the number of Aka molecules is given by:

$$\dot{A} = k_{syn}$$

On average, $k_{syn}*\Delta t$ Aka molecules are produced per time step. Stochastic variation was introduced using a Poisson distribution. In addition, the cell the molecule belongs to, as well as the position

within its membrane and the angle of the molecule, are chosen randomly. The Matlab 'rand' function was used as random generator.

Degradation

Analogous to synthesis, degradation in the model implies the removal of molecules from membranes, which does not distinguish between proteolytic degradation and recycling. Degradation is assumed to be a first order reaction:

$$\dot{A} = k_{deg} * A$$

Since $k_{deg} * \Delta t <<< 1$, the probability that a molecule is degraded during a time step is calculated as $k_{deg} * \Delta t$. It is assumed that a molecule cannot be degraded if it is, directly or indirectly, bound to a molecule from another cell. In addition, it is assumed that degradation is more efficient for smaller complexes. Thus, the degradation constant decreases with the number of molecules in a complex.

Diffusion

Lateral diffusion for a single molecule is being modeled by (Einstein, 1905; Erban *et al.*, 2007):

$$\Delta x = \sqrt{2D\Delta t} * \xi$$

The x-position denotes the horizontal distance from the TCJ, D is the diffusion constant and ξ is a random number from a normal distribution with mean 0 and standard deviation 1. The y-position is the vertical distance from the bottom of the membranes. To calculate Δy, the same equation was used as for Δx, but another random number was used. D was assumed to be the same for each direction, independent of the orientation of the molecules or of a chain-like complex of molecules. Within the TCJ, Δx was set to 0. A complex was assumed to be at the TCJ if it contained at least one molecule of each of the three cells. The diffusion coefficient was assumed to be proportional to n^{-1} (Landau and Lifshitz, 1959), where n denotes the number of Aka molecules in the complex. For non-junction boundaries Neumann (zero-flux) boundary conditions were used. At the junction, Neumann boundary conditions were used for multimeric complexes containing molecules from two different cells, whereas single molecules or complexes containing molecules from only one cell were allowed to diffuse through it freely.

Rotational diffusion was calculated in the same way as lateral diffusion, but in order to calculate the change in angle, a different diffusion constant was used, which is proportional to n^{-3} (Landau and Lifshitz, 1959).

Binding

Two Aka molecules are assumed to bind if they touch, *i.e*. if their centers are two radii apart at most. In the case of complexes, it is assumed that binding can only occur at the ends of the complexes. Thus, an Aka molecule can bind two other Aka molecules at most, resulting in the formation of homomultimeric complexes (stacks) with a valence of two for each Aka molecule, as depicted in Figure 7A. There is no limit to the length of the stack, except that it has to fit within the membrane. Binding is assumed to be possible between molecules of the same cell, as well as from different cells. Upon binding, the angle of the new complex is the weighted mean of the angles of the former two components. The model does not include cooperative effects associated with multivalent binding, but assumes that Aka molecules associate independently of the size of pre-existing complexes.

Dissociation

Binding is assumed to be reversible. If complexes are split into two parts, the probability that they rebind, is very close to 1 (Andrews and Bray, 2004). Therefore, analogous to (Andrews and Bray, 2004), it was assumed that dissociation leads to a displacement of the products, so that the distance between the two centers of molecules at the ends of the complexes becomes two times the radius of an Aka molecule plus the unbinding distance.

Dissociation was assumed to be a first order reaction. For each binding event, the probability for unbinding was calculated by:

$$P_{dis} = k_{dis} * \Delta t$$

As for degradation, this approximation was used since $k_{dis} * \Delta t <<< 1$.

For the simulations shown in Figure S6 (D-F), the dissociation constant differed for complexes at and outside the TCJ. Complexes were defined to be localized at the TCJ if they contained molecules from three different cells. For the case in which Aka is only produced by two neighboring cells, complexes were defined to be at the TCJ if their centers were at most one Aka diameter removed from the TCJ.

Representation of Aka molecules and complexes

Aka monomers are assumed to be spherical. Homomultimeric Aka complexes are assumed to behave as stiff rods. At the TCJ, molecules are not allowed to overlap, except for limited overlap that results from diffusion or dissociation and that is followed by binding during the subsequent time step. Outside the junction this limitation is not imposed, so that, if the parameters in the model allow for it, there is no limit to the number of molecules that can accumulate at the membranes outside the TCJs. Since this

is not realistic, simulations were stopped as soon as the bicellular membranes contained 300,000 molecules.

Parameter values

The parameter values used are listed below. The diameter of an Aka protein was estimated based on the minimal radius of a sphere containing the mass of the protein (350 kDa). The unbinding distance was taken to be equal to the Aka diameter, which is very similar to the value used in (Andrews, 2005). Lateral diffusion constants of proteins in membranes are typically between 0.001 and 0.2 $\mu m^2/s$ (reviewed in Sanderson, 2012). The lower limit of this range was selected for Aka, since septate junction proteins tend to have very low mobility (Oshima and Fehon, 2011) and Aka may bind to septate junction proteins. The lateral and rotational diffusion constants are usually physically coupled in a prescribed way. However, in the case of Aka, binding to septate junction proteins could hinder rotation, especially in the case of multimeric complexes. Therefore, it is hard to estimate the rotational diffusion constant and we chose 0.01 rad^2/s. However, this value does not appear to be critical, since increasing it by a factor of 10 as well as setting it to 0 did not lead to a significantly different enrichment ($p>0.4$ for each case). The height of TCJs varies between cell types. We chose 10 μm and chose the same value for the width of membrane modeled, which is half of the bicellular membrane. Doubling and halving these values, while concurrently doubling and halving the rate of synthesis, did not significantly change the enrichment factor ($p>0.1$ in each of the four cases).

The other parameter values are not known for Aka protein and were fitted by hand for maximum enrichment within a reasonable time frame. Even though the production rate and the degradation rate appear to be within a reasonable range (Hirschberg *et al.*, 1998; Moal and Fernandez-Recio, 2012), the degradation rate found in this way is likely to be too high. In the model, the time spent by Aka monomers at the membrane is on the order of seconds, whereas the time spent at the plasma membrane measured for a number of transmembrane proteins is on the order of minutes (Koenig and Edwardson, 1997; Goh *et al.*, 2010). This could, in addition to the limited robustness, be viewed as another argument why this simple model is not sufficient to fully explain the localization behavior of Aka protein. However, the lack of robustness appears to be inherent, since robustness did not change when modeling details, such as the random generator used, were modified. Note that the parameter values may change drastically when additional factors are included in the model. If, for example, the hypothesis of increased binding stability at the TCJ is included into the model by decreasing the dissociation rate by a factor of 10 for complexes at the TCJ and the degradation and production rate are decreased by a factor of 50, the resulting enrichment is similar to that obtained by the simple model and the dynamics are only about 20% slower.

Parameter	**Value**
Estimated Aka protein diameter	0.01 µm
Unbinding distance	0.01 µm
k_{syn}	250 s^{-1}
k_{deg}	0.2 s^{-1} (n=1); 0.15 s^{-1} (n=2); 0.1 s^{-1} (n=3); 0.0 s^{-1} (n>3)
k_{dis}	0.02 s^{-1}
D	$0.001*n^{-1}$ $\mu m^2 s^{-1}$
D_{rot}	$0.01*n^{-3}$ $rad^2 s^{-1}$
Membrane height	10 µm
Membrane width (half)	10 µm

Parameters used for the simulations.

Controls

For reliable simulations, the time step needs to be small enough that molecules bind if their paths cross each other. On the other hand, the time step needs to be large enough, so that the above approximation for diffusion can be used, in which the velocity of a molecule at a previous time step is being ignored. The latter is the case if the following requirement has been fulfilled (Gillespie and Seitaridou, 2013):

$$\Delta t \gg \frac{mD}{k_b T}$$

, where m denotes the mass of a molecule, D the diffusion constant, k_b the Bolzmann constant and T the temperature. We chose Δt such that $\sqrt{2D\Delta t}$ is about 0.1 times the binding distance, leading to a value of $5*10^{-4}$ s in most simulations. In this case, Δt is at least 10^{12} times larger than $(mD)/(k_bT)$ and is thus clearly large enough to use the approximation (Gillespie and Seitaridou, 2013). In order to test whether Δt is also small enough, we decreased it by a factor of 10 and found that this decreased the enrichment by about 5%, thereby not changing any of our conclusions. The different processes were modeled in the same order as listed above. Changing this order did not alter the enrichment by more than 1%, as long as the change did not lead to an artifact in the sense that molecules can overlap so much in the TCJ that they do not bind any more during the next time step. This artifact was not seen in the basic model.

In addition to these technical controls, we also checked whether the model is consistent with our experimental result that Aka production in three adjoining cells is required for the accumulation of Aka at the TCJ. When Aka production in the model was limited to two cells only, there was indeed no accumulation of Aka at the TCJ (data not shown). Since we propose that Aka protein-specific features are also essential, we performed the same test for a slight variation of the model, in which Aka

complexes are selectively stabilized at the TCJ. In this case, Aka production is still required in the three adjacent cells (Figure S6D-F).

Analysis

Enrichment at the TCJs (e) was calculated as follows:

$$e = \frac{N_j}{N_m} * \frac{X_{max}}{d_A}$$

, where N_j and N_m denote the number of Aka molecules at the TCJ and at the bicellular membrane, respectively, X_{max} denotes the simulated membrane width, and d_A denotes the diameter of an Aka molecule.

In order to test whether results are significantly different from the basic model, a *t*-test was performed comparing the enrichment after 2.5 hrs of simulated time.

Supplemental References

Andrews, S.S. (2005). Serial rebinding of ligands to clustered receptors as exemplified by bacterial chemotaxis. Phys Biol *2*, 111-122.

Andrews, S.S., and Bray, D. (2004). Stochastic simulation of chemical reactions with spatial resolution and single molecule detail. Phys Biol *1*, 137-151.

Einstein, A. (1905). Über die von der molekularkinetischen Theorie der Wärme geforderte Bewegung von in ruhenden Flüssigkeiten suspendierten Teilchen. Annalen der Physik *322*, 549-560.

Ejsmont, R.K., Sarov, M., Winkler, S., Lipinski, K.A., and Tomancak, P. (2009). A toolkit for high-throughput, cross-species gene engineering in Drosophila. Nature Methods *6*, 435-437.

Erban, R., Chapman, S.J., and Maini, P.K. (2007). A Practical Guide to Stochastic Simulations of Reaction-Diffusion Processes. arXiv:0704.1908 [q-bio.SC]

Gillespie, D., and Seitaridou, E. (2013). Simple Brownian Diffusion - An Introduction to the Standard Theoretical Models (Oxford, UK, Oxford University Press).

Goh, L.K., Huang, F., Kim, W., Gygi, S., and Sorkin, A. (2010). Multiple mechanisms collectively regulate clathrin-mediated endocytosis of the epidermal growth factor receptor. The Journal of Cell Biology *189*, 871-883.

Hirschberg, K., Miller, C.M., Ellenberg, J., Presley, J.F., Siggia, E.D., Phair, R.D., and Lippincott-Schwartz, J. (1998). Kinetic analysis of secretory protein traffic and characterization of golgi to plasma membrane transport intermediates in living cells. The Journal of Cell Biology *143*, 1485-1503.

Koenig, J.A., and Edwardson, J.M. (1997). Endocytosis and recycling of G protein-coupled receptors. Trends Pharmacol Sci *18*, 276-287.

Landau, L.D., and Lifshitz, E.M. (1959). Fluid Mechanics., Vol 6 (Oxford, Pergamon).

Le, T., Liang, Z., Patel, H., Yu, M.H., Sivasubramaniam, G., Slovitt, M., Tanentzapf, G., Mohanty, N., Paul, S.M., Wu, V.M*., et al.* (2006). A new family of Drosophila balancer chromosomes with a w-dfd-GMR yellow fluorescent protein marker. Genetics *174*, 2255-2257.

Luschnig, S., Moussian, B., Krauss, J., Desjeux, I., Perkovic, J., and Nusslein-Volhard, C. (2004). An F1 genetic screen for maternal-effect mutations affecting embryonic pattern formation in Drosophila melanogaster. Genetics 167, 325-342.

Moal, I.H., and Fernandez-Recio, J. (2012). SKEMPI: a Structural Kinetic and Energetic database of Mutant Protein Interactions and its use in empirical models. Bioinformatics *28*, 2600-2607.

Pedelacq, J.D., Cabantous, S., Tran, T., Terwilliger, T.C., and Waldo, G.S. (2006). Engineering and characterization of a superfolder green fluorescent protein. Nat Biotechnol *24*, 79-88.

Sanderson, J.M. (2012). Resolving the kinetics of lipid, protein and peptide diffusion in membranes. Mol Membr Biol *29*, 118-143.

Tonning, A., Hemphälä, J., Tång, E., Nannmark, U., Samakovlis, C., and Uv, A. (2005). A transient luminal chitinous matrix is required to model epithelial tube diameter in the Drosophila trachea. Developmental Cell *9*, 423-430.

Wisniewski, J.R., Zougman, A., Nagaraj, N., and Mann, M. (2009). Universal sample preparation method for proteome analysis. Nature Methods *6*, 359-362.